

Structure and transport of alongshelf currents across the southern flank of Georges Bank during late summer, 1982

RONALD J. SCHLITZ^{*1}, JAMES P. MANNING^{*} and KESTON W. SMITH[°]

Abstract--An array including seven moorings was in place between 10 August and 25 September, 1982 on southern Georges Bank. This was the second setting in cooperation with the Warm-Core Rings Experiment (WCR II). Ten of the records from the Vector Averaging Current Meters (VACMs) were complete. Short-term drifters with window-shade drogues at 10 m were launched and recovered seaward of the shelfbreak (200 m) to document flow of shelf water across bathymetry. Winds were available for this period from NOAA buoy 44003 at the southwestern corner of Georges Bank near the array. The major structure in the subtidal flow is an alongshelf maximum toward the west (mean speed $\sim 27 \text{ cms}^{-1}$ with bursts often $> 30 \text{ cms}^{-1}$) at the shelfbreak front ($\sim 100 \text{ m}$); the shelfbreak jet. The first two modes in empirical orthogonal analysis of the cross-bank structure contain 82% of the variance. Mode 1 is associated with the large-scale alongshelf current and is partially correlated with local winds. Mode 2, generally not correlated with wind, may be generated by features initiated by the Gulf Stream. The current record at the northern periphery of the warm eddy or remnant of a warm-core ring has a mean velocity of 5 cms^{-1} toward the east for the period, opposite the general circulation over the shelf. Elsewhere the circulation over the shelf seemed minimally affected even with the proximity of the offshore feature.

A mean estimate for volume transport of shelf water during the period is $0.83 \pm 0.2 \text{ sv}$ with

^{1*}NOAA/NMFS/NEFSC, Woods Hole, MA 02543

[°]Professional and Technical Services, Inc., Norfolk VA, 23502

periods of greater than 1 sv related to NE winds leading by six hours. While a bias is possible due to undersampling of the velocity field, this mean value and variability during late summer are higher than previously reported estimates for transport of shelf water. This is primarily due to the additional contribution of the shelfbreak jet near the 100 m isobath. Confidence limits for the transport were calculated by two independent methods, geometric weighting and block estimation by universal kriging.

Keywords: Wind-driven currents; Volume transport; Current meter data; Hydrography; Georges Bank; Southern flank

INTRODUCTION AND MOTIVATION FOR EXPERIMENT

One source of mortality for planktonic species is removal from a favorable habitat (e.g., Iles and Sinclair, 1982). Among the hypothesized physical mechanisms for dislocation of pelagic organisms from Georges Bank are alongshore transport into the Middle Atlantic Bight and entrainment of shelf water by Gulf Stream warm-core rings, i.e., advection of shelf water beyond the normal position of the shelf/slope front and subsequent loss from the coastal ocean. The organism associated with the entrained shelf water would eventually be within a hostile environment for survival. The overall importance of this loss on subsequent recruitment of year-classes of fish has been discussed often, always including caveats. For example Cohen et al. (1986) attempt to partition various physical effects on recruitment of haddock for Georges Bank. They conclude that different advective processes, including entrainment by warm-core rings, could dominate at different times. Their analysis was complicated because a strong storm with high winds occurred concurrently with the passage of a warm-core ring. Direct measurements showing the intensity and frequency of entrainment and distribution of shelf larvae beyond the shelf break south of Georges Bank were not available to help

their interpretation. On the other hand, flow along the isobaths from Georges Bank to the Middle Atlantic Bight results in an unequivocal loss for populations of zooplankton on the southern flank. This is a continuous mechanism operating throughout the year on plankton within the water column. Mean speeds along isobaths of $10\text{-}20\text{ cm s}^{-1}$ would remove plankton from the southern flank in approximately a week unless counteracted by biological processes. The balance between these various mechanisms affecting mortality of zooplankton and ichthyoplankton remains an open question.

Georges Bank is a broad, shallow section of continental shelf that separates the deeper Gulf of Maine from the main body of the Atlantic Ocean. While the mean circulation is generally clockwise around the bank continuing into the Middle Atlantic Bight, some turning into Great South Channel is shown during the stratified season (Manning and Beardsley, 1996). Butman and Beardsley (1987) present a seasonal cycle for circulation around Georges Bank, peaking in late summer. However, Limeburner and Beardsley (1996) could not confirm the seasonal cycle in circulation from a series of drifters with drogues at 5 m and 50 m. Also, no drogue at the 50 m level recirculated around Georges Bank. Significant fluctuations at higher frequencies occur due to tides, time-varying winds, and variations in density structure. Changes in the position of both the tidally mixed front (in the stratified season) and the shelf/slope front along the southern flank result in deviations from the classical gyre-like flow. These may provide the primary mechanism for seasonal and interannual differences in the retention and loss of ichthyoplankton and their prey.

The details of frontal dynamics as summarized by Flagg (1987) include several processes. These include a seasonal migration of the front bankward from winter through the summer, the presence of the cold band in the deep water just shoreward of the shelf/slope front in spring and

summer, the potential effects of warm-core rings throughout the year, and other small scale processes such as calving, the detachment of parcels of shelf water into slope water (Garvine et al., 1988). However, on the southern flank, few reported experiments of long duration have sufficient spatial resolution to determine the structure of the alongshelf currents or to calculate volume transports. Nearby, toward the west, Beardsley et al. (1985) report on an array of current meters south of Nantucket for 13 months. Also Manning and Beardsley (1996) discuss a synthesis of many individual settings of current meters across Great South Channel and the southern flank of Georges Bank.

A series of cruises was completed by NMFS in coordination with the Warm-Core Ring project sponsored by NSF. During one cruise (June 1982), a Multiple Opening Closing Net Environmental Sensing System (MOCNESS) with an opening of one square meter sampled plankton at stations on the continental shelf and within entrained shelf water associated with ring 82-B. These stations were in the Middle Atlantic Bight off the Delmarva Peninsula. LeBlanc (1986) reports that 12 species of larval fish were identified within entrained shelf water seaward of the 200 m isobath. For example, the mean standard lengths for *P. Triacanthus* (butterfish) of 4.3 mm and *M. bilinearis* (silver hake) of 4.9 mm are sizes associated with recently hatched larvae (unfortunately comparative samples from the other cruises in the series were lost). Schlitz (1999) concludes from examining the temperature-salinity properties of ring-entrained water that the predominant source is along the outer continental shelf seaward of the cold band (Houghton et al., 1982), but at times includes a contribution from the seaward side of the cold band.

Besides the shipboard physical and biological sampling completed during the Warm-Core Ring project, two moored arrays were set along and across the shelf break to examine the interaction

between rings and shelf water. The first of these arrays (WCRI) was in place between 15 April and 1 July 1982 south of New England. Ramp (1989) reports on current variability in relation to the radiation of barotropic topographic waves from ring 82-B. He also concludes from temperature measurements that two months are needed to restore the shelf/slope front to a "normal" position after passage of a warm-core ring. Ramp (1986) proposes two mechanisms that could trigger entrainment of shelf water; horizontal shear instability along the front formed between the ring water and shelf water and wakes resulting from Rossby waves.

The second array (WCRII) sampled currents and temperature along the southern side of Georges Bank between 10 August and 25 September, 1982. The placement of WCRII was determined after sea-surface temperatures derived from AVHRR data indicated that a warm-core ring was present in the area. Subsequently, AVHRR images showed that the feature was more likely a complicated structure on the northern periphery of the meandering Gulf Stream rather than an isolated ring. The feature interacted continuously with the main Gulf Stream located toward the south during deployment (Figure 1). Detailed interpretation of a time series of AVHRR data was hampered by clouds.

This report emphasizes the structure of alongshelf flow, effects of wind on the circulation, and estimates of variations in transport during WCRII. The interval of time covered by this moored array, although short, is important since maximum stratification generally occurs during late summer and the total alongshelf flow should also reach a maximum (Butman and Beardsley, 1987).

DATA

WCRII was deployed on the southern flank of Georges Bank between 10 August and 25

September, 1982. The array had both alongbank and crossbank components (Figure 2). Basic information for each instrument and corresponding statistics are presented in Table 1a. All moorings were recovered but the current meter at site 4 lost when wire rope parted during retrieval of the instrument. All other sites returned records from the instrument near the surface (10 m) except site 3 in which the tape failed to advance. In addition subsurface instruments were at site 3 (40 m, 100 m, and 305 m) and site 6 (35 m and 85 m). Vector-averaging current meters (VACMs) were used at each location to record a vector-averaged velocity and instantaneous temperature every 15 minutes. All data were processed by the Woods Hole Oceanographic Institution using the standard data analysis system for oceanographic time series. The 15-minute samples were checked for gaps and bad points and hourly time series were generated.

An additional check was made on these data for known tides. The most energetic currents on Georges Bank occur at the semi-diurnal period (M2), increasing in amplitude from the southern flank to the northern edge (e.g., Manning and Beardsley, 1996; Moody et al., 1984). The amplitudes, semi-major and semi-minor axes, and phases of currents at the M2, O1, K1, N2, and S2 periods were determined for each instrument in the array. M2 values are consistent with previous results ranging from 8 cm s^{-1} at the edge of the continental shelf to 53 cm s^{-1} at the northern end of the array near the tidally mixed front. For example, site 5 nearly corresponds to site K in Moody et al. (1984). The semi-major axes of the tidal ellipses from these sites agree to within 1%, and the semi-minor axes to within 10%. The orientations of the tidal ellipses differ by $1.1E T$. Although the results are expected, it gives additional confirmation of the quality and consistency of these data.

Low-passed time series were then calculated using a digital filter with a half-point at 33 hours,

PL33 (Flagg et al., 1976), which removes tides (Table 1b). The east and north components of velocity were rotated onto principal axes to determine the direction of low-frequency variability (Table 2a). Also axes relative to the local overall mean alongshore current at each instrument were determined for further analyses (Table 2b).

Winds for the region were taken from NOAA Buoy 44003, at 40E48' N , 68E30' W (Figure 2). Anemometers were situated at 5 m above the surface as part of the standard General Service Buoy Payload (GSBP). On this system both wind speed and direction were sampled at 1 Hz and averaged every 8.5 minutes. These data were then averaged to hourly time series. Also, peak hourly gusts were recorded. Wind stress was calculated from the hourly time series (see Manning and Strout, this issue, for a summary of methods).

Temperature and salinity profiles were collected using a continuously recording Conductivity/Temperature/Pressure (CTD) instrument during cruises that set and recovered the moorings. Water samples were collected at selected depths during casts. Salinities, which were determined by a precision conductive salinometer, were then used to check the calibration of conductivity data. Temperature, salinity, and density sections along the mooring line are shown in Figure 3. Shelf water is defined by salinities < 34 ; based on the range of salinities generally found on Georges Bank inside the shelfbreak front (Schlitz, 1999).

During the cruise of *R/V Albatross IV* to set the moored array, five surface buoys drogued at 10 m were launched and tracked for short periods. Each consisted of a window-shade approximately 220 ft² (21 m²) in area, attached by thin line to a high-flyer at the surface, approximately 1 ft² (0.09 m²) in cross-sectional area. The purpose was to follow the offshelf movement in an entrainment associated

with a warm-core ring. The resulting data are summarized in Table 3. Four of the five drogues (D1, D3, D4, D5) were launched in a surface layer of shelf water at oceanic depths greater than 200 m. The fifth, the easternmost (D2), was always in water with salinity > 34 near the boundary between shelf water and slope water. Temperature and salinity characteristics at the drogues were determined through a series of additional CTD casts.

A T-S diagram for all stations in the region is presented in Figure 4. The demarcation between shelf water and slope water occurs at a maximum temperature of about 21.7°C for these data.

RESULTS

Subtidal temperature and currents

The low-passed temperatures from thermistors on each current meter are shown for the duration of the moored array (Figure 5). Some noteworthy features are within the time series. Temperatures at 10 m's from sites one and two, located along the ~ 325 m isobath, decrease markedly early in the record. Maximum temperatures for both, 24.7°C at site 1 and 25.2°C at site 2, occur at the beginning of the record. These temperatures can be associated with water from the warm feature of the Gulf Stream (Figure 4). One CTD station taken within this feature produces a limb on the T-S diagram with temperatures > 25 °C. Temperatures then decrease to minimums of 15.6°C at site 1 and 16.8°C at site 2. These temperature changes result from inflow of cooler shelf water coincident with southward recession of the feature. The inverse trend happens at site 3 (record at 40 m), warming from 8.5°C to 17.2°C as the cooler shelf water from an earlier entrainment of shelf water is displaced. The near-surface record at site 6 has variability typical of measurements near the shelfbreak front (e.g.,

Flagg, 1987). Also a characteristic signature of the cold band, temperatures around 10°C, is seen at a depth of 35 m on site 6. Although site 7 was positioned to sample changes in the slope water regime associated with variability in loss of shelf water by entrainment, only shelf water persisted until the end of the record. Resolution of spatial variability at a short scale above the thermocline between sites 3 and 7 was not possible with the loss of the record at 10 m on mooring 3.

The overall means of low-passed currents during the WCRII array are shown in Figure 2 and Table 2. Currents at sites 5 and 6 on the shelf follow the general trend of the local mean topography. Largest velocities, 27 cm s^{-1} toward 250°E T and 19 cm s^{-1} toward 255°E T, were found on mooring 6 at depths of 10 m (6-1) and 35 m (6-2) respectively. The means at sites 1 and 2, both near the 325 m isobath, suggest convergence between the moorings during two months. Site 1 is opposite the overall shelfwide flow toward the southwest resulting from the influence of the circulation associated with the Gulf Stream interaction. The velocities at site 3 show considerable variation with depth. Influence of the local topography is possible since the mooring is located on the continental slope between Powell and Lydonia Canyons (Figure 2). The mean at site 7 is small and toward the north.

Individual currents at each instrument in the array can be seen from the progressive vectors (Figure 6). Flow is generally parallel to the bathymetry toward the southwest at all locations except site 7 in 895 m of water where net movement was small, and site 1 described above. Intensification of flow in deeper water over the southern flank is clearly portrayed. The largest movements toward the southwest are at 10 m and 35 m depths for site 6 at 100 m on the southern flank. These are the only locations where low-passed currents exceeded 30 cm s^{-1} during periods of low wind. This structure has only recently (Linder and Gawarkiewicz, 1998, Pickart et al., 1998, Manning et al., 1999) been

called the shelfbreak jet though clearly it is a permanent part of the alongshelf circulation (e.g., Flagg, 1977). The core of the current is generally centered between 100 m and 120 m in the Middle Atlantic Bight (Linder and Gawarkiewicz, 1998), shallower than the large increase in bottom-slope at approximately the 200 m isobath, defined as the shelfbreak for this region.

Specific drogues were followed between 15 hours and 70 hours (Table 3). D2 was recovered after a series of four CTD stations taken at the position of the drogue showed only slope water (surface salinity of 34.76 and temperature of 22.31EC at the final station). D1 was also recovered after leaving shelf water. D3 - D5 were recovered earlier than planned due to unanticipated needs of another project. Except for a single station alongside D5 with a salinity at the surface of 32.95, increasing to 33 at 5 m, all salinities for shelf water were greater than 33 at the drogues indicating a source near the shelfbreak front. In addition, the near-surface temperatures associated with these salinities were everywhere greater than 19.5EC and predominately greater than 20EC (Figure 4). These T-S values are found near the surface above the 100 m isobath as shown in Figure 3.

Mean velocities over the duration of each drogue are shown in Figure 7, superimposed on the surface temperature field from an AVHRR image during the period. Low-passed velocities at 10 m from each current meter for the hour closest to the AVHRR transit are also included. The overall drift determined from the drogues appears decoupled from the currents over the southern flank of Georges Bank during this time. Excepting D5, which is close to the 34 isohaline at a western boundary of entrained shelf water, there is no cross-isobath flow of shelf water potentially associated with the nearby circulation of water originating from the Gulf Stream. The mean direction of D3 is consistent with the northern edge of a cyclonic ringlet described by Kennelly et al. (1985), albeit at a lower speed.

There is no further information in the currents to confirm this. D1, D2, and D4 moved opposite the mean regional circulation.

Wind-driven response

Wind-driven response of currents on the southern side of Georges Bank shows significant variability during the summer. This association can be seen through examples. On 25-26 August 1982 “strong” SW-W winds (hourly averages >15 kt (7.7 ms^{-1} , 0.1 Pa) for 14 hours including three hours with $\$20$ kt (10.3 ms^{-1} , 0.18 Pa)) caused a response above the thermocline along the southern flank consistent with Ekman forcing (Figure 8). Surface currents rotated toward the south at each location, first at site 7 where the mean current was low. During this period, maximum currents at sites 5, 6, and 7 exceeded 30 cms^{-1} in the upper layer, suggesting significant southward excursions (>26 kmd^{-1}) for water on the southern flank of Georges Bank. Spin-up time coincides reasonably with the initiation of Ekman velocity at the surface, 7-8 hours for this latitude. Although speeds for wind at 7.7 - 10.3 ms^{-1} may not seem high in the yearly cycle for Georges Bank, the NOAA National Data Buoy Center (NDBC) (unpublished data) calculates an average wind speed of 3.8 ms^{-1} during August at buoy 44003 for data collected between 1977 and 1983. Also, the average of hourly peak gusts for August was 4.1 ms^{-1} for data collected between 1981 and 1983. So this burst of southwesterly winds was at least double the mean condition from the time series at 44003.

On this and two other occasions these wind-driven offshore flows in the upper layer coincided with return flow at depth below the shelfbreak front. These three events are labeled in the bottom panel of Figure 9a where periods of northeastward wind stress forced southward flow at instrument 6-1 with northward flow at 6-3. Details are shown in Figure 9 b-d. At the beginning of each episode the total

low-passed current at 6-1 begins to rotate cyclonically from the mean southwesterly direction. This rotation is understood as the vector summation of the general alongshelf current and adjustment of the current vector near the sea surface following an Ekman response to the onset of wind. As the event progressed and the wind continued rotating toward the east, flow with an onshelf component developed at 6-3 when the wind stress was between 070E T and 105ET. Each instance was accompanied by a rise in temperature consistent with warmer slope water offshore at this depth (Figure 5).

This reversal of flow at depth was persistent enough to be captured in the spectral statistics. The coherence calculations between the north component of velocity at 6-1 and 6-3 showed a phase difference of approximately 180E, using overlapping segments of 10 days and averaging over four frequency bands. Also, the statistical relationship between eastward wind and the northward current at 6-3 was in phase with a transfer function of $84 \pm 42 \text{ cms}^{-1}\text{Pa}^{-1}$, following Bendat and Piersol (1986) for confidence intervals. Although this presumed upwelling does not happen continuously, the transfer function is only one third that near the surface ($259 \pm 70 \text{ cms}^{-1}\text{Pa}^{-1}$), and the statistics are not strongly significant due to limited degrees of freedom (10), the process represents an additional subtle intermittent flow across isobaths.

Wind stress was calculated for 15E T intervals in direction, and spectral quantities between wind and currents at mooring 6 estimated to determine the component of the wind most effective in driving the near-surface currents over the southern flank. Significant values resulted for certain rotations, again noting the limitation in the number of degrees of freedom. The north/south variability recorded at 6-1 was best correlated with no rotation of the east/west wind (Figure 10a) in the 1-2 day band. The phase of approximately $180 \pm 25\text{E T}$ at the 95% confidence level indicates a southward

flow responded to a west wind (eastward stress). East/west variability recorded at 6-1 was most coherent with the northeast/southwest component of the wind (Figure 10b). In this instance the phases are insignificantly different from zero showing northeastward wind stress driving eastward flow and southwestward wind stress driving westward flow. These results are consistent with Noble et al. (1985) for data collected across four years on the southern flank of Georges Bank. The period of this east/west process was longer (3-5 days vs. 1-2 days) but not as effective with transfer functions of $136 \pm 55 \text{ cms}^{-1}\text{Pa}^{-1}$ versus $259 \pm 70 \text{ cms}^{-1}\text{Pa}^{-1}$.

Estimates of residual velocities from the tracks of drogues required removal of slippage (Geyer, 1989; Allen, 1995) and the large wind-driven component seen in the currents at 10 m from the mooring sites. First, the transfer functions between current and wind at 7-1, $-177 \pm 64 \text{ cms}^{-1}\text{Pa}^{-1}$ and $355 \pm 129 \text{ cms}^{-1}\text{Pa}^{-1}$, were applied to the eastward and northward wind stress, respectively, to estimate the southward and eastward components of wind-driven flow. The slippage between the window-shade and flow was then needed.

Previous estimates of slippage for drifters (Geyer, 1989; Allen, 1995) are between 0-6 cms^{-1} depending on both configuration of the drifter and the wind/wave conditions. Since slippage for a window-shade drifter with a high-flyer has apparently never been measured, a middle value of 3 cms^{-1} in the downwind direction was chosen for the correction. Because the wind was oriented in the alongshelf direction during the drifter deployment, uncertainty in the magnitude of slippage should only minimally affect any estimate of crossbank residual velocity.

The resulting residuals (total velocity - wind-driven component - slippage) show a mean flow toward the southern flank of Georges Bank at about 5 cms^{-1} (Figure 11) for the drifters set near the

200 m isobath. The direction for D3 remains compatible with a location at the northern side of a small cyclone in the entrained shelf water. Consistency in the directions of the three drogues (D1, D2, D4) and the residual current for site 7 at 10 m for the same period is surprising, particularly with the warm anticyclonic feature in close proximity. Note in particular that the direction for D5 reverses substantially once the wind-driven component was removed.

EOF analysis

Empirical orthogonal functions showing the variance in a group of time series were determined for the portion of the array across the shelf (sites 5, 6, 3, and 7). The first two modes for structure of the alongshelf component of low-passed currents, illustrated in Figure 12, account for 82% of the total variance, 63% in mode 1 and 19% in mode 2. Mode 1 represents the large scale alongshelf flow, peaking for the record at 10 m in the shelfbreak jet, site 6-1. Mode 2 is governed by the records at depths greater than 10 m found off the shelf and represents a response to features induced by the Gulf Stream. Highest amplitudes are found at site 3 for the depths of 100 m and 305 m. Figure 13a visually shows correlation between the mode 1 and the alongshore winds. Coherence calculations are significant in a band from 1.3 to 3.6 days for mode 1 but suffer from low degrees of freedom. The significant correlation between alongshore winds and mode 1 is expected since mode 1 is comprised mainly of shallower time series over the shelf.

Two events dominate the series in Figure 13; the northeastward stress between 25-26 August 1982 that affected both modes and the southwestward stress between 6-8 September 1982 for mode 1. These results generally agree with the interpretation of the data from NSFE79 (Beardsley et al., 1985) which separates flow over the continental shelf, partially driven by the wind, from that at the edge

of the shelf. The current record at 10 m for the seaward mooring of Beardsley et al. (1985) located in 810 m of water contributes to mode 2 associated with passage of warm-core rings. The current at site 7 of the present study in 895 m of water was part of flow over the shelf, mode 1.

Transport variability

Transport of water along the continental shelf can be estimated for the duration of the array. To place confidence limits on volume transport, two independent methods for calculations were developed and are presented in Appendix 1. The first is based on assigning areas to each velocity record, a traditional method for estimating volume transport. Confidence limits for the traditional estimates are produced under the assumption that the spatial distribution of velocity is locally Gaussian with a constant variance and a mean which changes in time. The variance of the velocity distribution in each area is estimated from the time-averaged variance of the instruments about the area. A local mean of velocity is estimated from the record of an instrument found within the area. The neighborhood scheme was defined by taking the closest adjacent instruments to the instrument used for the estimate of mean, both horizontally and vertically if other instruments were present. Instrument 6-2 was added to the neighborhood of instrument 5-1 and instruments 3-3 and 3-4 were added to the neighborhood of instrument 7-1 to factor in the variance in current due to depth at those sites. The second estimation is by block universal kriging. For the kriging estimates it is assumed that the velocity structure at each time step is the sum of a linear function and an unknown spatially-correlated noise term. The transport estimator for each time is restricted to be a constant linear combination of data from that time, with coefficients of the linear combination from that period chosen to minimize the prediction error. Confidence intervals for the transport are derived from the additional assumption that the prediction

error of the linear predictor has a Gaussian distribution.

Figure 3 shows the areas associated with the first method superimposed on the two CTD sections. The calculations were limited to a region approximating shelf water, salinities < 34 . Likewise kriging was limited to shelf water through pseudo-topography that treats the 34 isohaline as a solid boundary. Extension of the area for mooring 5 into shallower water was based on drifter tracks (Limeburner and Beardsley, 1996) showing that mean flow toward the southwest is found at depths shallower than the 50 m isobath. The outer boundary is more problematic for the first CTD section since shelf water extends beyond mooring 7. However the speeds are generally low as seen in the drogoue tracks, so minor underestimates for shelf water were possible. Although the east and north components of velocity were reasonable approximations to the alongbank and crossbank directions, transports were also calculated based on the direction of the mean alongbank current for each location. Sensitivity of the estimates to local topography could be bounded in this way.

The estimated transports of shelf water shown in Figures 14 and 15 are based on the distributions of salinity at the beginning and end of the time series (Case 1 and Case 2). Corresponding weights and confidence limits computed for the geometric and kriging methods are in Table 4. Kriging is considered less subjective since weights are not determined by positions of instruments alone and account for the covariance structure of the currents. The mean estimated transport August-September, 1982 based on all estimates is 0.83 ± 0.2 sv. This value is generally higher than transports reported earlier (Manning and Beardsley, 1996; Beardsley et al., 1985) for the area.

The time series of alongbank transport shows four periods (Figure 16) when all estimates were greater than 1 sv. These were on 22 August, 29 August, 9 September, and 18-19 September.

Visually, all were associated with moderate NE winds blowing < 12 hours earlier at speeds between 7.2 ms^{-1} and 8.2 ms^{-1} (14 -16 kt), indicating rapid alongshelf response of transport to southwesterly wind stress over the southern flank of Georges Bank. The representativeness of these observations within the time series was investigated by determining the maximum correlation between the alongshelf transport of shelf water and the vector of wind stress. The result was a correlation of 0.66 between volume transport and wind stress toward 211E T leading by 6 hours. This correlation is well above the value for significance at the 95% confidence level, 0.37, suggesting a primary role for wind in forcing variability of transport along the southern flank of Georges Bank during summer. The total gain for these conditions is $4.89 \pm 1.28 \text{ svPa}^{-1}$, calculated as covariance between wind stress and transport divided by the variance of wind stress.

DISCUSSION

Vertical structure of wind-driven response

The WCRII array demonstrates that low-frequency episodes of alongshelf wind stress toward the northeast are effective in driving the current field off the southern flank of Georges Bank. Although contemporaneous and correlated, the vertical response at 6-3 cannot be directly forced by wind through an Ekman layer. Under homogeneous conditions, a maximum calculated Ekman depth for the three events is 55m well above the depth of 6-3, 85 m. Also, Werner (1999) concludes that the Ekman response is mainly trapped above thermocline on the southern side of Georges Bank. One explanation for the vertical structure comes from recent modeling. Greenberg et al. (1997) formulated a three-dimensional, harmonic, finite-element model forced at low frequency by wind peaking at 0.1

Pa. Results show that a combination of direct Ekman forcing and pressure-gradient response results in a significant divergence in the surface currents near the 60 m isobath on the southern side of Georges Bank. They also note upwelling (i.e., return flow at depth to surface flow off the shelf) is particularly strong for the southern side of Georges Bank. In addition, the modeled field of deep velocity near site 6 has a component across the bathymetry into shallower water. A region of convergence in flow near the bottom occurs at oceanic depths of about 60 m on the southern flank. Therefore, continuity is maintained by vertical motion in this area.

This flow across isobaths in response to winds from the southwest gives an intermittent process that adds nutrients to the shelf from locations at the base of the shelfbreak front. Results from many studies (e.g., Schlitz and Cohen, 1984) show that mean nitrogen content below 75 m on the southern side is higher than levels on Georges Bank, particularly in summer. However, any quantitative estimate of the potential flux from this process is beyond the present scope.

Residual velocity of drogues

An AVHRR image for 16 August was contoured to emphasize frontal features (Figure 11). Residual flow for drogues D1, D2, and D4 toward the shelfbreak front at $\sim 5 \text{ cms}^{-1}$ is clearly shown. These and the concurrent residual at site 7 suggest that convergence at the shelfbreak front leads to flow toward the shelf in the surface layer at that time. The 20EC isotherm at the surface is within the gradient associated with the shelfbreak front and crosses site 6 indicating that the shelfbreak jet was near the 100 m isobath there. The speed of $\sim 5 \text{ cms}^{-1}$ is higher than the findings of Churchill and Manning (1997). They report a convergence of 2 cms^{-1} onto the shelfbreak front in the same area using sets of clustered drifters. The 21EC isotherm nearly enclosed cooler water off the shelf at D3

consistent with a cyclonic ringlet (Kennelly et al., 1985). Demarcation between flow affected by warm circulation appears to coincide with the 23EC isotherm and salinities >34.6 (Figure 4). The residual motion of D5 is not easily explained from available data.

Transport variability

The mean transport of shelf water (salinity < 34) calculated here, 0.83 ± 0.2 sv, is higher than transports reported earlier for the area. This may be expected since the moorings were in place during the time of maximum stratification on Georges Bank. Butman et al. (1987) discuss the seasonal cycle of currents on Georges Bank, primarily seen as baroclinic adjustment to the density changes during the stratified season, although Limeburner and Beardsley (1996) could not confirm the cycle. The only other reported estimate of directly measured transport along the southern flank of Georges Bank is by Manning and Beardsley (1996) for the period 27 July - 18 November, 1985. A mean value of 0.421 sv inside the 100 m isobath results from multiplying the low-passed velocity by the cross section over which the velocity acts. The same calculation for a subset of these data, 1 September - 31 October, produces 0.428 sv. Information is not available about the water types carried along the southern flank within the flow. Farther to the west, Flagg (1977) estimates a transport of 0.4 sv based on three hydrographic sections adjusted with interpolated currents at 30 m from current meters. The raw mean estimates of 0.401 sv, inside the 100 m isobath, and 0.218 sv, outside the 100 m isobath, were adjusted based on potential sources of error. These data were collected during the New England Shelf Dynamics Experiment, 27 February - 3 April, 1974. A different analysis by Beardsley et al. (1976), using the same measurements of currents and adding one additional record from the preceding year gives 0.168 sv inside the 100 m isobath. The reasons for the difference are not clear. Finally the

Nantucket Shoals Flux Experiment (NSFE79) gives 0.383 ± 0.069 sv at depths between 40 m and 120 m over the 13 month time series without any detectable seasonal variations.

Here the four separate estimates for transport, based on two salinity sections and two independent statistical models, are consistent. Questions remain about potential bias in the estimates due to undersampling of the velocity field. For example the currents for one depth at 5-1 are used to represent a substantial weight in the box method. There are no contemporaneous data with which to consider potential bias. Speculation about the magnitude of an error in transport can be conducted in the following way. Under the assumption that the basic physical processes remain within narrow bounds for summer seasons and alongshelf scales are long on Georges Bank, vertical shear collected nearby at the same isobath during an equivalent time for a different year can be used as a surrogate. Such data were collected during the GLOBEC II experiment in 1997. An Acoustic Doppler Current Profiler (ADCP) mounted on a tripod was located in 61m of water on the southern flank of Georges Bank between 16 January and 20 August 1997. The location (40E 42.9N, 68E 24.4W) was about 64 km toward the west-southwest of site 5. A mean vertical distribution of alongshelf currents was determined for the first 20 days of August, based on a vertical resolution of 1 m for the currents from the ADCP. This mean profile was adjusted to match the time series of velocity in the direction of the mean current at 5-1. Then estimates of transport were calculated by the geometric method. The resulting transports are 0.63 ± 0.13 sv for Case 1 and 0.74 ± 0.15 sv for Case 2. The decreases in the estimates of transport are 0.1 sv for Case 1 and 0.1 sv for Case 2. Similar calculations are not well suited to universal block kriging. Under the geometric method shear correction can be interpreted

statistically as an adjustment for a known bias in the velocity measurement. Due to spatial interdependence of the weighting scheme in the kriging calculation, it is not clear how to interpret the results of an adjustment to the kriging estimates for such a bias. Notwithstanding a limitation to only the geometric method for the calculation, the 12% - 15% reduction in transport estimates for Cases 1 and 2 are within the confidence intervals.

SUMMARY

The WCRII array on the southern flank of Georges Bank was designed to investigate interaction of shelf waters with warm-core rings originating from the Gulf Stream. Due to the complex structure of a meander and eddy-like feature of the Gulf Stream instead of a detached ring (Figure 1), understanding of the intricacy of interactions was not possible through these data. However, influence of these features originating from the Gulf Stream was shown directly in two ways. The mean current at site 1 was toward 089E T at 5 cm s^{-1} from 10 August through 25 September, 1982, opposing the general circulation over the continental shelf. Concurrently temperatures at sites 1 and 2 steadily decreased from a maximum of 24.7EC at the beginning of the record to 15.6EC on 7 September while a meander of the Gulf Stream moved southeast away from the shelf, as interpreted from available AVHRR images. Also a mean one-dimensional convergence was indicated along the 325 m isobath between sites 1 and 2, inferring undefined cross-isobath flow, possibly due to meandering of the shelfbreak front in response to anticyclonic circulation off the shelf (Figure 11). In addition shelf water, previously entrained, was present well seaward of the normal position for the shelfbreak front.

The major feature in the circulation pattern over the southern flank of Georges Bank for this period was the shelfbreak jet, captured in the current records at site 6 in 100 m of water. The mean

speeds at 6-1 (10 m) and 6-2 (35 m) were 27 cms^{-1} and 19 cms^{-1} toward the WSW respectively. The velocities of Beardsley et al. (1985) for the shelf south of Nantucket, Manning and Beardsley (1996), and Butman et al. (1982) for the southern flank of Georges Bank, are approximately 50% of these results. However the period covered by the present measurements was shorter than the others and was at the time of maximum stratification in the seasonal cycle. More recently Linder and Gawarkiewicz (1998) geostrophically calculate velocities of 20 cms^{-1} - 30 cms^{-1} for the shelfbreak jet in the Middle Atlantic Bight. Also, residual flow for drifters, drogued with window-shades at 10 m and located offshore in entrained shelf water at an oceanic depth of 200 m, was toward the shelfbreak front at $\sim 5 \text{ cms}^{-1}$.

Empirical orthogonal analysis clearly divided the alongshelf flow into a component over the southern flank of Georges Bank (63% of the total variance) that is part of the large-scale circulation along the continental shelf and a fraction in deeper water (19% of the total variance) forced by meanders and eddies of the Gulf Stream.

Even though winds for the period were less than 10 ms^{-1} except for three hours on 26 August 1982, there were significant wind-driven responses in the circulation above the southern flank. Overall both alongshelf and across-shelf variability of currents were best correlated with alongshelf variability in wind stress at lags of approximately 6 - 8 hours.

During the short burst of winds from the SW at speeds approaching 10 ms^{-1} , the surface currents at sites 5-1, 6-1, and 7-1 rotated cyclonically toward the south consistent with an Ekman response in the upper layer perturbing the mean alongshelf current. Maximum southerly speeds were greater than 30 cms^{-1} . During three instances of SW winds, the response at site 6 showed flow toward

the south at 6-1 in response to the wind. This was accompanied by northward flow at 6-3 toward a divergence in flow at the surface near the 60m isobath on Georges Bank, observed in results from modeling (Greenberg et al., 1997). This intermittent upwelling of slope water near the shelfbreak is a potential source of nutrients for the southern flank of Georges Bank since the mean direction for wind in the summer is from the SW.

Estimates of volume transport for the duration of the moored array were calculated by a geometric estimation method that echoes the classical method and block universal kriging. Hydrographic sections completed during the setting and recovery of the array were used to define shelf water as the region with salinity < 34 . An additional comparison was made between estimates calculated from the east component of velocity applied to the entire section and a local alongshelf direction determined from the mean at individual records. At the 95% confidence level all estimates overlap leading to an overall estimate of 0.83 ± 0.2 sv. The alongshelf transport responded at a lag of 6 hours to NE winds blowing at moderate speeds. On four occasions transports in excess of 1 sv were estimated for NE winds blowing between 7.2 ms^{-1} and 8.2 ms^{-1} (14-16 kt).

APPENDIX 1

Because of the sparsity of our data over the region covered by the transport calculations confidence intervals to account for prediction error in transport due to spatial undersampling were produced. Unfortunately an accounting for all small scale variability and biasing is not possible due to placement of instruments during the experiment. Analysis that accounts for variation in the velocity field on a scale smaller than the spacing of the instruments would require reconstruction of the velocity fields through assimilation of the data into a circulation model, beyond the present scope.

Transport was estimated by a simple geometric estimation method and by block universal kriging, a procedure of linear prediction with minimum error. The geometric method approximates the transport by partitioning the cross section over which the transport is being calculated into polygonal subregions, each subregion containing one current meter. This method is used extensively in oceanography for transport estimates (e.g., Churchill and Berger, 1998, Mercier and Speer, 1998). Here, as in earlier calculations, the polygons are oriented rectangles intersected with the bottom topography. A partition is chosen so that the flow through each polygon is reasonably homogeneous. The contribution of each instrument to the transport estimate is the area of the subregion containing the instrument. Transport estimates by kriging use a least-squares fit of a polynomial to the data at each time step and subsequent spatial analysis of the residual.

For a cross section containing N instruments sampling in unison let $Z(t)=(Z_1(t),Z_2(t),\dots,Z_N(t))$, where $Z_k(t)$ denotes the speed of the water in the direction of the transport calculation sampled by the instrument located at x_k, y_k at time t . Let $S(t)$ denote the transport at time t , the integral of the speed over the region of transport. Let T be the number of samples gathered by the instruments with samples

gathered at times $t=1, 2, \dots, T$.

Confidence intervals for transport estimates computed by the geometric method were constructed under the assumption that the distribution of current in each subregion is Gaussian with constant variance but a mean which changed in time. The constant variance for each subregion was estimated by averaging the sample variance with neighboring instruments at each time step over the length of the record. The estimates of variance for each polygon should be larger than the actual variance since the instruments used to estimate the variance lie in a larger region than the individual polygon. See Table A1 for the neighborhoods and dimensions of rectangles constructed for the present data.

Under the assumption that the flow through each polygon is Gaussian with constant variance and a time-dependent mean, the two sided a confidence interval for the mean estimate, $\mu_k(t)$, of the transport at time t through polygon k is:

$$\left(Z_k(t) + s_k N^{-1}((1 - \alpha) / 2), Z_k(t) + s_k N^{-1}((1 + \alpha) / 2) \right)$$

where s_k is the estimated standard deviation of the signal in the k 'th polygon

$$s_k = \frac{\sum_{t=1}^T \sqrt{\sum_{j \in \text{Neighbors}(k)} \left(Z_j(t) - \frac{\sum_{i \in \text{Neighbors}(k)} Z_i(t)}{\# \text{Neighbors}(k)} \right)^2}}{T}$$

and N^{-1} is the inverse of the standard normal distribution. The transport estimate is:

$$S^{est}(t) = \sum_{k=1}^n Z_k(t)(\text{Area of subregion } k)$$

with a confidence interval:

$$\left(S^{est}(t) + \sum_{k=1}^n (\text{Area } k) \mathbf{s}_k N^{-1}((1 - \mathbf{a}) / 2), S^{est}(t) + \sum_{k=1}^n (\text{Area } k) \mathbf{s}_k N^{-1}((1 + \mathbf{a}) / 2) \right)$$

Estimates of transport were also calculated by block kriging, a statistical procedure for estimating spatial integrals from point sampled data. Standard procedures for kriging are designed for data assumed to be collected at a single time. This is largely because kriging was originally developed for geological data (e.g., mineral concentrations) which are collected on a time scale much shorter than the time scale in which the distributions change. For oceanographic time series modifying traditional kriging to deal with the rapid temporal dynamics is necessary. Only the methods that were specifically adapted for the kriging calculation on the present time series are presented. Details of the kriging derivation are found in section 3.4 of Cressie (1993).

For the kriging calculations data are assumed to be of the form:

$$Z(x, y, t) = \sum_{j=1}^m B_j(t) f_j(x, y) + \mathbf{d}(x, y, t)$$

where f_j are known constant functions, B_j are time-dependent unknown coefficients, and \mathbf{d} is a

stationary random process with zero mean which has a distinct realization at each sampling time. The units of f and d are the same as the units of the observations. The transport estimates presented here use a quadratic mean function:

$$\begin{aligned} f_1(x, y) &= 1, f_2(x, y) = x, f_3(x, y) = y, f_4(x, y) = xy, \\ f_5(x, y) &= x^2, f_6(x, y) = y^2 \end{aligned}$$

The predictor of the transport is assumed to be a constant linear combination of the data, that is

$$\text{predictor}(S(t)|Z) = \sum_{k=1}^N \mathbf{1}_k Z_k(t).$$

Finding the minimal error predictor and confidence intervals by kriging requires knowledge of a variogram, $\gamma(x,y)$. The variogram is the function specifying the spatial structure of the variance of the d process,

$$\mathbf{g}(x, y) = \frac{\text{var}(\mathbf{d}(x_0 + x, y_0 + y) - \mathbf{d}(x, y))}{2}.$$

γ was estimated by a least squares fit of a linear function in x and z to the entire collection of sampled residuals, $\mathbf{d}(x_k, y_k, t) = Z(x_k, y_k, t) - \sum_{j=1}^m \hat{B}_j(t) f_j(x_k, y_k)$. $\hat{B}(t)$ is chosen

independently at each time step to minimize

$$\sum_{k=1}^N \left(Z(x_k, y_k, t) - \sum_{j=1}^m B_j(t) f_j(x_k, y_k) \right)^2$$

The confidence intervals for the transport estimates by this method of kriging are based on a mean-squared error of prediction and an assumption that the transport is drawn from a Gaussian distribution. Because of the assumption that d does not change in time, the error in prediction is independent of time and is

$$\mathbf{s}_E^2 = E\left[\left(S(t) - \sum_{k=1}^N \mathbf{I}_k Z_k(t)\right)^2\right]$$

where $S(t)$ is the true transport at time t . From the Gaussian assumption, the two-sided a confidence interval on the prediction of transport, $\hat{S}(t) = \sum_{k=1}^N \mathbf{I}_k Z_k(t)$, is

$$\left(\hat{S}(t) + \mathbf{s}_E N^{-1}((1 - \mathbf{a}) / 2), \hat{S}(t) + \mathbf{s}_E N^{-1}((1 + \mathbf{a}) / 2)\right).$$

The details of the calculation of minimal variance σ^2 from the data, the f_i and σ^2 can be found in Cressie (1993), section 3.4. A summary of the parameters estimated for the kriging calculation can be found in Table A1. Figure A1 shows the results of these calculations.

REFERENCES

Allen, A. A. (1995) The determination of slippage of drifters and the leeway of search and rescue targets using Interocean S4 EMCMS. Proceedings of the IEEE Current Meter Conference 1995.

Beardsley, R. C., W. C. Boicourt, and D. V. Hansen (1976) Physical oceanography of the Middle Atlantic Bight. In: *Middle Atlantic Continental Shelf and the New York Bight*, Special Symposium, **2**, Limnology and Oceanography, M. Grant Gross, Allen Press, Lawrence, Kansas, 441 pp.

Beardsley, R. C., D. C. Chapman, K. H. Brink, S. R. Ramp, and R. Schlitz (1985) The Nantucket Shoals Flux Experiment (NSFE79). Part I: A basic description of the current and temperature variability. *Journal of Physical Oceanography*, **15**, 713-748.

Bendat, J. S. and A. G. Piersol (1986) Random data. J. Wiley and Sons, New York, 566pp.

Butman, B. and R. C. Beardsley (1987) Long-term observations on the southern flank of Georges Bank. Part I: A description of the seasonal cycle of currents, temperature, stratification, and wind stress. *Journal of Physical Oceanography*, **17**, 367-384.

Butman, B., J. W. Loder, and R. C. Beardsley (1987) The seasonal mean circulation: observation and theory. In: *Georges Bank* R. H. Backus and D. W. Bourne, MIT Press, Cambridge, Massachusetts,

593 pp.

Butman, B., R. C. Beardsley, B. Magnell, D. Frye, J. A. Vermersch, R. Schlitz, R. Limeburner, W. R. Wright, and M. Noble (1982) Recent Observations of the mean circulation on Georges Bank. *Journal of Physical Oceanography*, **12**, 569-591.

Churchill, J. H. and T. J. Berger (1998) Transport of Middle Atlantic Bight shelf water to the Gulf Stream near Cape Hatteras. *Journal of Geophysical Research*, **103**, 30605-30621.

Churchill, J. H. and J. P. Manning (1997) Horizontal convergence and dispersion over the southern flank of Georges Bank, ICES CM 1997/T:31.

Cohen, E. B., D. G. Mountain, and R. G. Lough (1986) Possible factors responsible for the variable recruitment of the 1981, 1982, and 1983 year-classes of haddock (Melanogrammus aeglefinus L.) on Georges Bank. Northwest Atlantic Fisheries Organization, SRC. Document 86/110, Serial Number N1237. 27 pp.

Cressie, N. A. C. (1993) *Statistics for spatial data*. J. Wiley and Sons, New York, 900pp.

Flagg, C. N. (1987) Hydrographic structure and variability. In: *Georges Bank* R. H. Backus and D. W. Bourne, MIT Press, Cambridge, Massachusetts, 593 pp.

Flagg, C. N. (1977) The kinematics and dynamics of the New England Continental Shelf and shelf/slope front. Ph.D. thesis. Woods Hole Oceanographic Institution - Massachusetts Institute of Technology, WHOI Reference 77-67, Woods Hole, Massachusetts, 208pp.

Flagg, C. N., J. A. Vermersch, and R. C. Beardsley (1976) 1974 MIT New England Shelf Dynamics Experiment (March 1974) data report, part II: The moored array. MIT Technical Report 76-1, Massachusetts Institute of Technology, Cambridge, Massachusetts, 22pp.

Garvine, R. W., K. -C. Wong, G. G. Gawarkiewicz, R. K. McCarthy, R. W. Houghton, and F. Aikman III (1988) The morphology of shelfbreak eddies. *Journal of Geophysical Research*, **93**, C12, 15,593-15,607.

Geyer, W. R. (1989) Field calibration of mixed-layer drifters. *Journal of Atmospheric and Ocean Technology*, **6**, 333-342.

Greenberg, D. A., J. W. Loder, Y. Shen, D. R. Lynch, and C. E. Naimie (1997) Spatial and temporal structure of the barotropic response of the Scotian Shelf and Gulf of Maine to surface wind stress: A model-based study. *Journal of Geophysical Research*, **102**, 20,897-20,915.

Houghton, R. W., R. Schlitz, R. C. Beardsley, B. Butman, and J. L. Chamberlin (1982) The Middle Atlantic Cold Pool: Evolution of the temperature structure during summer 1979. *Journal of Physical*

Oceanography, **12**, 1019-1029.

Iles, D. and M. Sinclair (1982) Atlantic herring stock discreteness and abundance. *Science*, **215**, 627-633.

Kennelly, M. A., R. H. Evans, and T. M. Joyce (1985) Small-scale cyclones on the periphery of a Gulf Stream warm-core ring. *Journal of Geophysical Research*, **90**, C 5, 8,845-8,857.

LeBlanc, P. R. (1986) The distribution and abundance of larval fishes in shelf water entrained by warm-core ring 82-B. M.S. thesis. Southeast Massachusetts University, South Dartmouth, Massachusetts, 143 pp.

Limeburner, R. and R. C. Beardsley (1996) Near-surface recirculation over Georges Bank. *Deep-Sea Research II*, **43**, 1547-1574.

Linder, C. A. and G. G. Gawarkiewicz (1998) A climatology of the shelfbreak front in the Middle Atlantic Bight. *Journal of Geophysical Research*, **103**, 18,405-18,423.

Manning, J. P. and R. C. Beardsley (1996) Assessment of Georges Bank recirculation from Eulerian current observations in the Great South Channel. *Deep-Sea Research II*, **43**, 1575-1600.

Manning, J. P. and G. Strout (2000) Georges Bank Winds: 1975-1997. *Deep-Sea Research II*, accepted.

Manning, J. P., R. G. Lough, C. E. Naimie, and J. H. Churchill (1999) The effect of a slope water intrusion and shelfbreak jet on larval advection along the southern flank of Georges Bank, *ICES Journal of Marine Science*, accepted.

Mercier, H. and K. G. Speer (1998) Transport of bottom water in the Romanche Fracture Zone and the Chain Fracture Zone. *Journal of Physical Oceanography*, **28**, 779-790.

Moody, J. A., B. Butman, R. C. Beardsley, W. S. Brown, P. Daifuku, J. D. Irish, D. A. Mayer, H. O. Mofjeld, B. Petrie, S. Ramp, P. Smith, and W. R. Wright (1984) Atlas of Tidal Elevation and Current Observations on the Northeast American Continental Shelf and Slope. U.S. Geological Survey Bulletin 1611, Woods Hole, Massachusetts, 122 pp.

Noble, M., B. Butman, and M. Wimbush (1985) Wind-current coupling on the southern flank of Georges Bank: Variation with season and frequency. *Journal of Physical Oceanography*, **15**, 604-620.

Pickart R. S., D. J. Torres, T. K. McKee, M. J. Caruso, and J. E. Przystup (1999) Diagnosing a meander of the shelfbreak current in the Middle Atlantic Bight. *Journal of Geophysical Research*,

104, 3121-3132.

Ramp, S. R. (1989) Moored observations of current and temperature on the shelf and upper slope near ring 82B. *Journal of Geophysical Research*, **94**, 18071-18087.

Ramp S. R. (1986) The interaction of warm core rings with the shelf water and shelf/slope front south of New England. Ph.D. dissertation, University of Rhode Island, Kingston, Rhode Island, 137 pp.

Schlitz, R. J. (1999) The interaction of shelf water with warm-core rings. *Journal of Geophysical Research*, in revision.

Schlitz, R. J. and E. B. Cohen (1984) A nitrogen budget for the Gulf of Maine and Georges Bank. *Biological Oceanography*. **3**, 203-222.

Werner, S. R. (1999) Surface and bottom boundary layer dynamics on a shallow submarine bank: southern flank of Georges Bank. Ph.D. thesis. Woods Hole Oceanographic Institution - Massachusetts Institute of Technology, MIT/WHOI Reference 99-13, Woods Hole, Massachusetts, Massachusetts, 222pp.

TABLES

Table 1. Basic information for the second array of current meters set as part of the Warm-Core Rings Experiment (WRCII), 10 August - 25 September, 1982. Panel a. contains the basic statistics on the time series averaged to hourly samples. Panel b. contains statistics for low-passed data after filtering to remove tidal and inertial energy.

Table 2. Principal axes and mean values for the data collected as part of WRCII, 10 August - 25 September, 1982. Panel a. has the principal axes of low-passed currents. The direction for the major axis is arbitrarily chosen to correspond to the highest numerical value on the compass. For example the major axis for 5-1 is along 080-260E T. Panel b. has the overall mean speed and direction for each instrument in the array.

Table 3. Data for drifters launched and recovered during a cruise of *R/V Albatross IV*. Each drifter was drogued with a window-shade centered at 10 m.

Table 4. Weights used and mean estimates for transport of shelf water by the geometric method and universal block kriging for WRCII. Panel A. uses the salinity from the CTD section in August, 1982 (Case 1) to determine shelf water and Panel B. uses salinity from the CTD section in September, 1982 (Case 2).

Table A1. Coefficients used in the geometric method and universal block kriging for estimating transport from an array of velocities at individual points. Lambda (?) is the vector of coefficients for linear estimator of mean transport producing minimum error.

FIGURES

Figure 1. AVHRR image taken at 08:00 Z on 16 August 1982 for region south of Georges Bank showing interactions of the Gulf Stream. Positions of the array set for Warm-Core Rings II (WRCII) are shown for reference.

Figure 2. Locations for moored array set during Warm-Core Rings II (WRCII), 10 August - 25 September 1982 on southern flank of Georges Bank. Mean low-passed currents from each current meter and mean velocities from drogues are shown. Mooring locations are circles and launch points for drogues are squares. The designation at the head of the arrow corresponds to the depth in meters for the measurement. All drogues are at 10 m. Also shown is the position of NOAA data buoy 44003. Bathymetry is in meters.

Figure 3. Temperature (EC), salinity (psu), and density (σ_t) sections across the southern flank of Georges Bank. Figure 3a. is for data collected on 16 August, 1982 during the cruise on *R/V Albatross IV* to set the moored array. Figure 3b. is for data collected on 25 September 1982, during the cruise on *R/V Delaware II* to recover the array. Positions of individual instruments are also shown. The black lines indicate boundaries to areas assigned for transport calculations.

Figure 4. Temperature-Salinity diagram for CTD stations completed in the vicinity of moorings and drogues during the cruise on *R/V Albatross IV*.

Figure 5. Low-passed temperature records from thermisters on each current meter during WCR II, 10 August - 25 September 1982. Figure 5a. is for records at 10 m depth. Figure 5b. is for all deeper records.

Figure 6. Progressive vectors for velocities recorded at moorings during WCR II. The top panel is for records at 10 m depth and the bottom panel is for all deeper records. All velocities were first scaled by 0.1 (i.e. the distance shown is one tenth that which a water parcel would travel) to fit on one chart. Tidal excursions are shown by cross-shelf variability in the tracks. Note that the depth of each record in the lower panel is posted in italics at the end of the track. Bathymetry in meters is labeled on the upper panel.

Figure 7. AVHRR image taken at 08:00 Z on 16 August 1982 showing vectors for each current measurement at 10 m at the same hour (black), and overall mean velocity for drogues with window-shades centered at 10 m (blue). The boundary for shelf water can be approximated by the 22EC isotherm.

Figure 8. Low-passed currents at 10 meters for three sites across the southern flank of Georges Bank and low-passed wind stress at buoy 44003 for 26 - 27 August 1982. Wind speeds during the period were highest, $> 10 \text{ ms}^{-1}$, for the period of the array.

Figure 9. Low-passed currents at site 6 for depths of 10 and 85 meters and low-passed wind stress at

buoy 44003. Figure 9a. shows three events for which there was upwelling associated with SW winds. Figures 9 b-d. provide details of the interaction of currents and winds for individual events.

Figure 10. Coherence between wind and current contoured as a function direction of wind and period. Direction of wind is shown by the arrows. Only significant values of coherence are contoured. The phase angles (negative for wind leading current) and transfer functions, gain in $\text{cm s}^{-1} \text{Pa}^{-1}$, correspond to significant coherence only. The top panel is for the north/south component of current and the bottom panel for the east/west component of current.

Figure 11. Mean residual velocities for drogues after wind-driven component and slippage was removed. The mean velocities, with wind-driven component removed, over the same period at 10 m from the current meters are shown. Included is the mean wind stress for the period. Contoured temperature at the surface is for AVHRR data at 08:00 Z on 16 August 1982.

Figure 12. The first two empirical orthogonal modes calculated from the low-passed records of alongbank flow during WCRII, 10 August - 25 September 1982 containing 82% of the variance. Mode 1, 63%, is shown by red arrows and mode 2, 19%, is shown by green arrows.

Figure 13. Amplitudes of the first two empirical orthogonal modes and wind stress during WCRII., 10 August - 25 September 1982. The top panel with mode 1 visually shows partial correlation in response. The bottom panel with mode 2 shows low correlation except for one event on 25-26 August, 1982

which caused a significant response.

Figure 14. Alongshelf transport of shelf water for the period of WCRII, 10 August - 25 September 1982, estimated from the salinity distribution at the beginning of the period, 16 August (Case 1). The top panel shows estimates of the transport from the east/west component of velocity at each site by a geometric method and universal block kriging. The bottom panel shows estimates of the transport using the maximum mean velocity at each instrument and same methods. Confidence intervals at 95% level are vertical lines.

Figure 15. Alongshelf transport of shelf water for the period of WCRII, 10 August - 25 September 1982, estimated from the salinity distribution at the end of the period, 25 September (Case 2). The top panel shows estimates of the transport from the east/west component of velocity at each site by a geometric method and universal block kriging. The bottom panel shows estimates of the transport using the maximum mean velocity at each instrument and same methods. Confidence intervals at 95% level are vertical lines.

Figure 16. Comparison of alongshelf transports of shelf water for the period of WCRII, 10 August - 25 September 1982. The top panel contains the four estimates using the geometric method. The bottom panel has the four estimates using universal block kriging. All estimates are within the confidence limits of the individual time series as shown in Figures 14 and 15.

Figure A1. Time series of transport determined by a geometric method and universal block kriging for an array of current meters.

a. Basic Statistics

Site	Latitude		Longitude meters	Water Depth meters	Instrument Depth meters	Temperature in °C				Eastward speed in cms ⁻¹				Northward speed in cms ⁻¹				Speed in cms ⁻¹			
	N	W				mean	minimum	maximum	st. dev.	mean	minimum	maximum	st. dev.	mean	minimum	maximum	st. dev.	mean	minimum	maximum	st. dev.
1-1	40 06.9	68 49.3	337	10	20.1	15.9	24.7	2.2	4.9	-72.7	55.2	19.5	0.1	-59.8	57.9	18.5	24.5	0.5	72.9	12.1	
2-1	40 18.0	67 56.5	325	10	20.2	16.8	25.2	2	-6.1	-68.5	47.8	17.4	-2.2	-64	47.7	15.6	21.5	0.1	68.5	11.3	
3-2	40 22.2	67 33.1	323	40	14	8.5	20	2.2	-2.3	-46.7	33.1	11.6	1.2	-44.5	35.8	13.3	15.8	0.5	47.8	8.2	
3-3				100	12.9	9.7	14.3	0.4	-7.7	-40.6	24.2	10.4	0.8	-29.6	28.4	10.5	15.4	0.5	44	6.5	
3-4				305	6.7	5.6	9.3	0.6	-4	-30.1	14	7.7	-0.9	-35.9	24.2	7.3	10	0.4	35.9	5.4	
5-1	40 57.2	67 42.8	60	10	15	12.9	17.4	0.8	-12.2	-78.4	65.3	32.4	-6.8	-98.2	67.5	38.6	49.9	1.2	100.2	15.5	
6-1	40 34.9	67 35.5	100	10	17.4	10.6	22.7	2.1	-25	-89.5	38.1	24	-9	-77.8	61.9	31.1	43.6	0.6	89.7	18.5	
6-2				35	10.9	7.8	20.9	2.2	-18.4	-79.3	31.6	21.6	-4.6	-69	56.4	26.7	36	0.3	85.8	15.5	
6-3				85	10.8	8.1	13.3	1.1	-5.7	-47.5	37.6	19.4	-2.8	-54.5	45.4	21.4	28.2	1.6	57.9	9	
7-1	40 19.5	67 31.6	895	10	20.1	15	23.4	1.1	0	-49.3	71.2	16	0.8	-73.7	42.7	17.3	20.7	0.2	81.6	11.4	

b. Low-Passed Statistics

Site	Latitude		Longitude meters	Water Depth meters	Instrument Depth meters	Temperature in °C				Eastward speed in cms ⁻¹				Northward speed in cms ⁻¹			
	N	W				mean	minimum	maximum	st. dev.	mean	minimum	maximum	st. dev.	mean	minimum	maximum	st. dev.
1-1	40 06.9	68 49.3	337	10	20.1	16.9	24.7	2	5	-12.4	18.1	7.3	0.2	-15.4	12	4.4	
2-1	40 18.0	67 56.5	325	10	20.1	17.6	25	1.9	-6.7	-31.7	11.1	8.3	-2.2	-20.3	8.3	4.5	
3-2	40 22.2	67 33.1	323	40	14.1	9.6	17.3	2	-2.6	-15.6	7	4.8	0.9	-8.9	11	4.8	
3-3				100	12.9	12	13.5	0.3	-8.5	-24.7	7.2	5.4	0.6	-10.5	8	3.7	
3-4				305	6.7	6	7.6	0.4	-4.2	-21.4	9.1	5.7	-0.9	-3.6	2.6	1	
5-1	40 57.2	67 42.8	60	10	15	13.5	16.1	0.6	-12.5	-27.5	1.1	6.2	-6.8	-31	6.2	5.6	
6-1	40 34.9	67 35.5	100	10	17.6	14.4	21.4	1.8	-25.3	-46.3	-8.3	7.4	-9.1	-30.6	11	8.1	
6-2				35	11	8	15	1.4	-18.6	-33.3	-4.7	6	-5	-23.7	11.6	6.1	
6-3				85	10.9	8.9	12.9	0.9	-5.8	-17.7	9.7	5.2	-2.8	-9.5	5.7	2.9	
7-1	40 19.5	67 31.6	895	10	20.1	16.7	22.8	0.9	-0.7	-16	24.8	6.8	0.9	-29.4	17.3	7.9	

a. Principal Axes

Site	Latitude N	Longitude W	Water Depth meters	Instrument Depth meters	Principal Axes of the low-passed (PL33) time series		
					major axis cms ⁻¹	minor axis cms ⁻¹	angle compass notation: °T highest angle
1-1	40 06.9	68 49.3	337	10	7.4	4.5	274
2-1	40 18.0	67 56.5	325	10	8.3	4.3	278
3-2	40 22.2	67 33.1	323	40	5	4.7	213
3-3				100	6	2.7	241
3-4				305	5.7	0.9	267
5-1	40 57.2	67 42.8	60	10	6.2	5.6	260
6-1	40 34.9	67 35.5	100	10	9.4	5.6	321
6-2				35	6.2	5.8	326
6-3				85	5.5	2.7	254
7-1	40 19.5	67 31.6	895	10	6.9	6.9	352

b. Mean Speed and Direction

Site	Latitude N	Longitude W	Water Depth meters	Instrument Depth meters	Mean speed and direction	
					cms ⁻¹	° T
1-1	40 06.9	68 49.3	337	10	5	89
2-1	40 18.0	67 56.5	325	10	7.1	253
3-2	40 22.2	67 33.1	323	40	2.8	289
3-3				100	8.6	274
3-4				305	4.3	258
5-1	40 57.2	67 42.8	60	10	14.2	242
6-1	40 34.9	67 35.5	100	10	26.9	250
6-2				35	19.2	255
6-3				85	6.4	244
7-1	40 19.5	67 31.6	895	10	1	326

Summary of measurements for drogued drifters during Albatross IV 82-09

Drifter Number	Location of Launch		Location of Recovery		Begin		End		Overall Distance		Mean Drift		Bearing Deg T	Launch Depth M
	Latitude	Longitude	Latitude	Longitude	Date	Time (Z)	Date	Time (Z)	NM	KM	knots	cms ⁻¹		
D1	40° 30.74'	67° 11.16'	40° 33.34'	67° 09.94'	13-Aug-82	2038	16-Aug-82	1442	2.76	5.12	0.04	2.15	019	207
D2	40° 39.55'	67° 03.22'	40° 39.95'	67° 01.91'	13-Aug-82	2313	14-Aug-82	1410	1.07	1.99	0.07	3.67	068	205
D3	40° 20.37'	67° 17.38'	40° 13.45'	67° 25.71'	14-Aug-82	2021	17-Aug-82	1843	9.40	17.41	0.13	6.86	223	1546
D4	40° 25.59'	67° 16.75'	40° 26.45'	67° 13.85'	15-Aug-82	2008	17-Aug-82	0650	2.37	4.39	0.07	3.48	069	587
D5	40° 09.47'	67° 30.84'	40° 08.41'	67° 29.89'	17-Aug-82	0110	17-Aug-82	2022	1.28	2.38	0.07	3.48	145	1724

a. Case 1, August 1982

Record for Computation	Geometric Method Component of Velocity		Universal Block Kriging Component of Velocity	
	West	Mean Direction	West	Mean Direction
5-1	0.5250	0.5250	0.4283	0.4528
6-1	0.1524	0.1524	0.2562	0.1390
6-2	0.1660	0.1660	0.2446	0.3283
6-3	0.0042	0.0042	0.2657	0.2378
7-1	0.1524	0.1524	-0.1948	-0.1579
Mean Transport (sv)	0.6651	0.7302	0.9275	0.9330
95% Confidence Interval (sv)	0.1767	0.1823	0.2064	0.2255

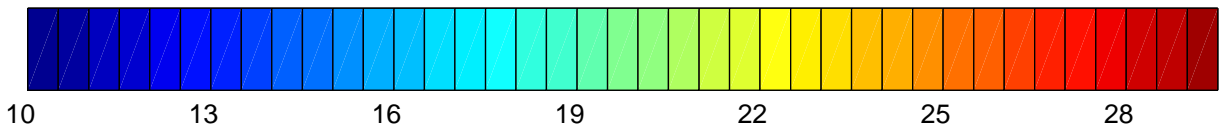
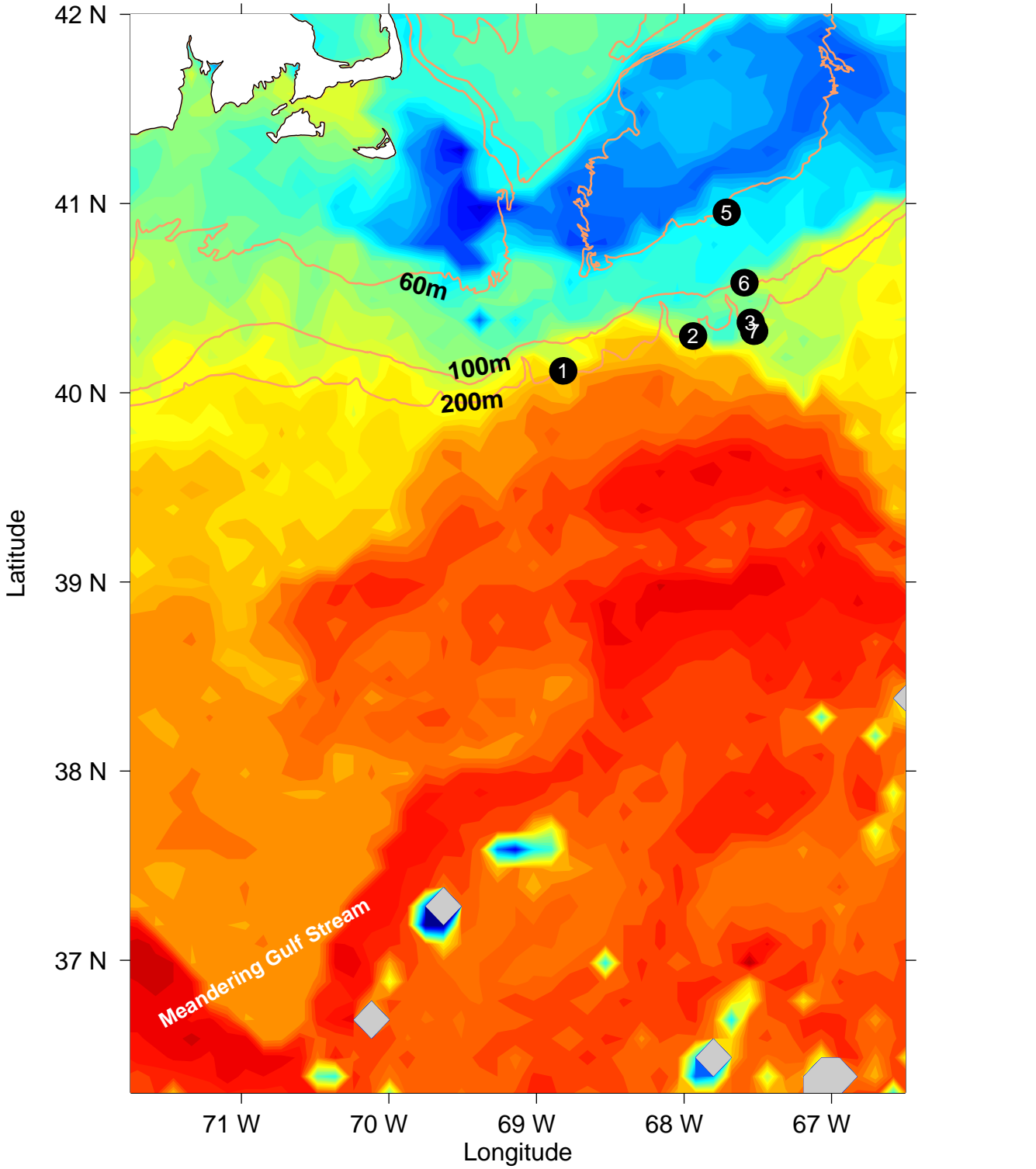
b. Case 2, September 1982

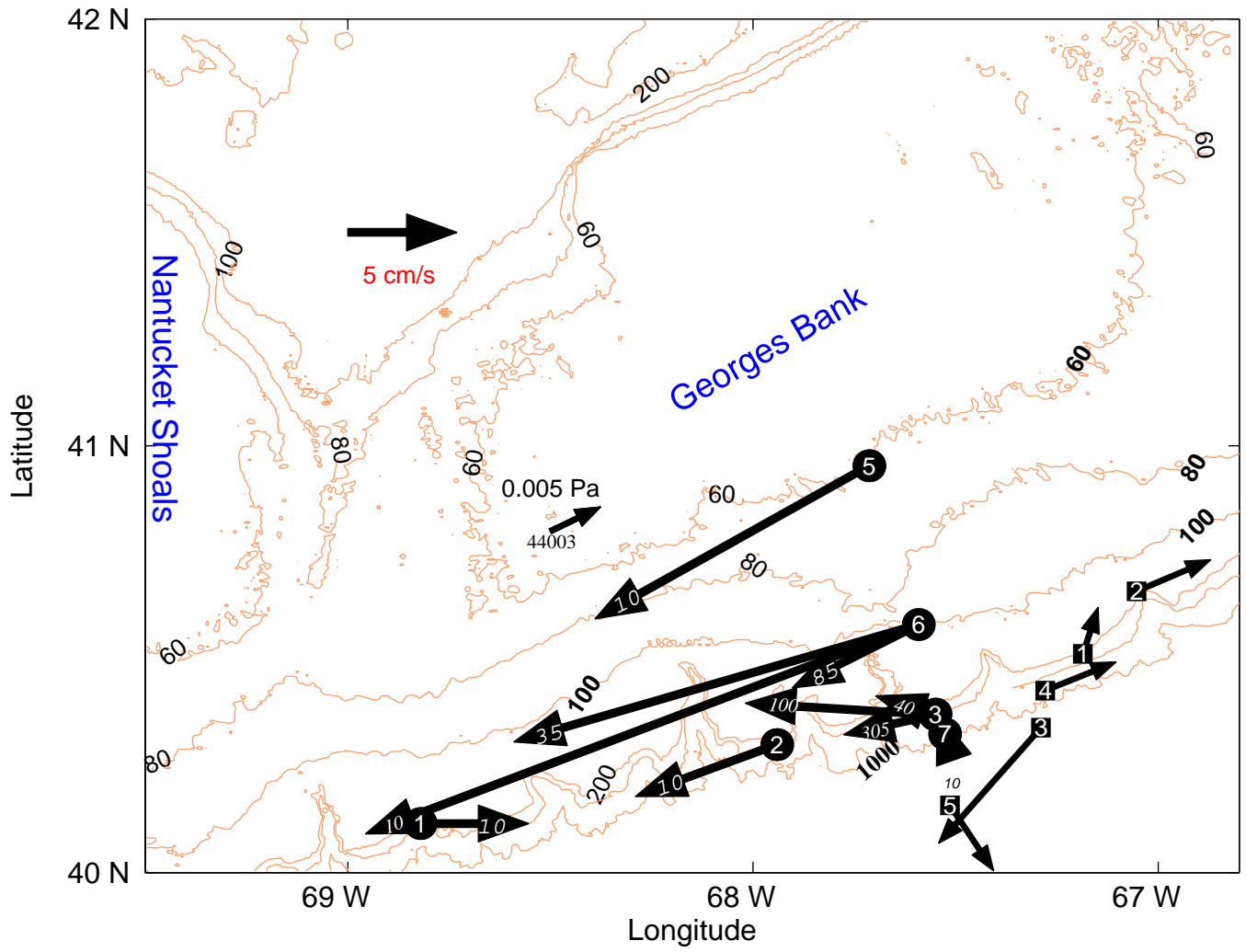
Record for Computation	Geometric Method Component of Velocity		Universal Block Kriging Component of Velocity	
	West	Mean Direction	West	Mean Direction
5-1	0.5035	0.5036	0.4436	0.4632
6-1	0.1319	0.1319	0.2753	0.1729
6-2	0.2108	0.2108	0.2296	0.3094
6-3	0.0485	0.0485	0.1790	0.1524
7-1	0.1052	0.1052	-0.1275	-0.0980
Mean Transport (sv)	0.7652	0.8371	0.8688	0.8871
95% Confidence Interval (sv)	0.1972	0.2034	0.1852	0.1991

Overall Mean Transport (sv) 0.83 ± 0.2

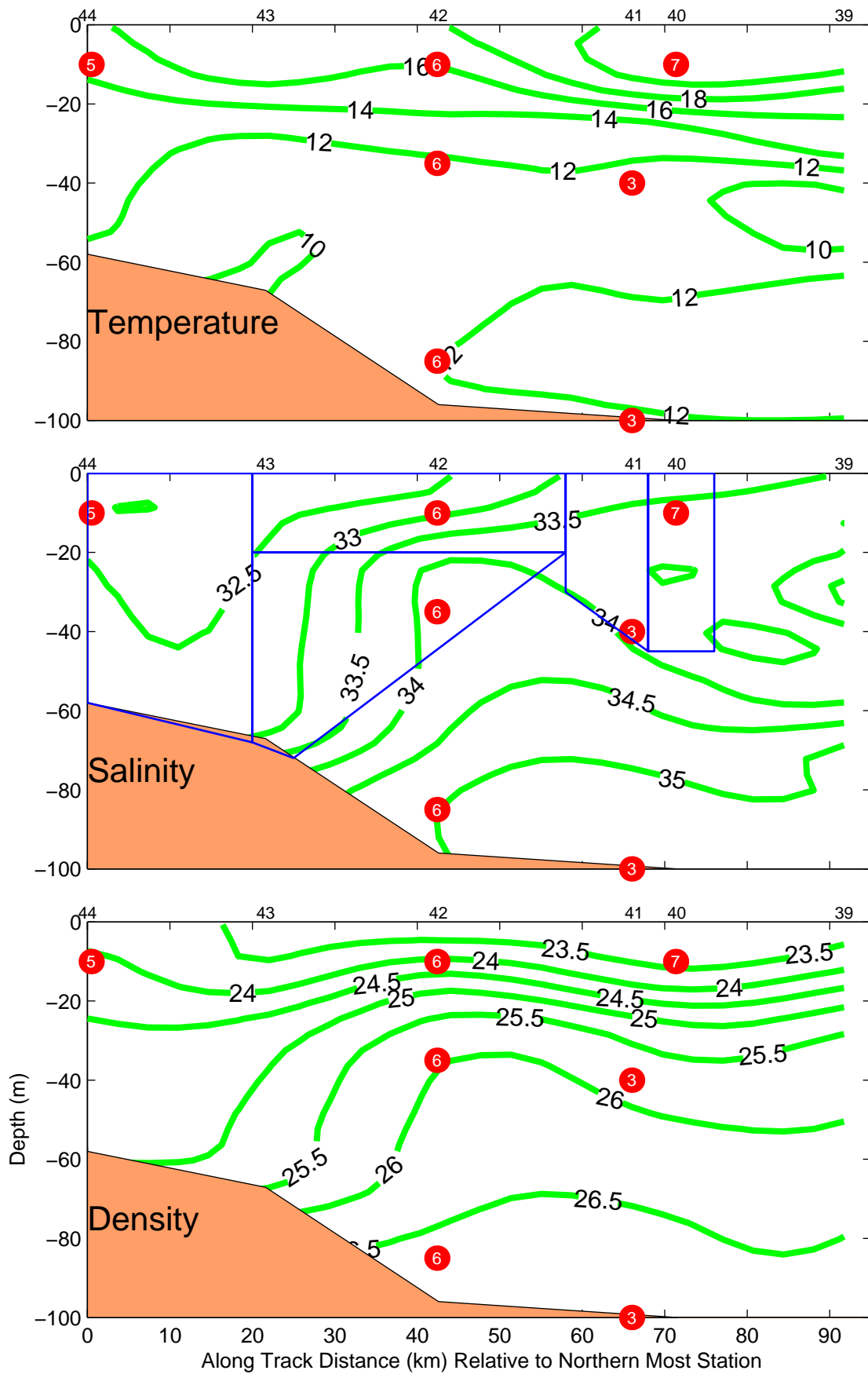
Instrument	Lambda (λ) for westward transport (kriging)	Neighborhood	Ratio of areas to total area for geometric estimate	Estimate of standard deviation
3-2	-0.104	{3-2, 3-3, 6-1, 7-1}	0.083	0.090
3-3	0.328	{3-2, 3-3, 3-4, 6-3, 7-1}	0.157	0.053
3-4	0.123	{3-2, 3-3, 6-3, 7-1}	0.139	0.055
5-1	0.233	{5-1, 6-1, 6-2}	0.213	0.074
6-1	-0.270	{3-2, 5-1, 6-1, 6-2, 7-1}	0.062	0.103
6-2	0.317	{3-2, 5-1, 6-1, 6-2, 6-3}	0.103	0.100
6-3	0.240	{3-3, 5-1, 6-2, 6-3}	0.110	0.071
7-1	0.134	{3-2, 3-3, 3-4, 7-1}	0.135	0.053

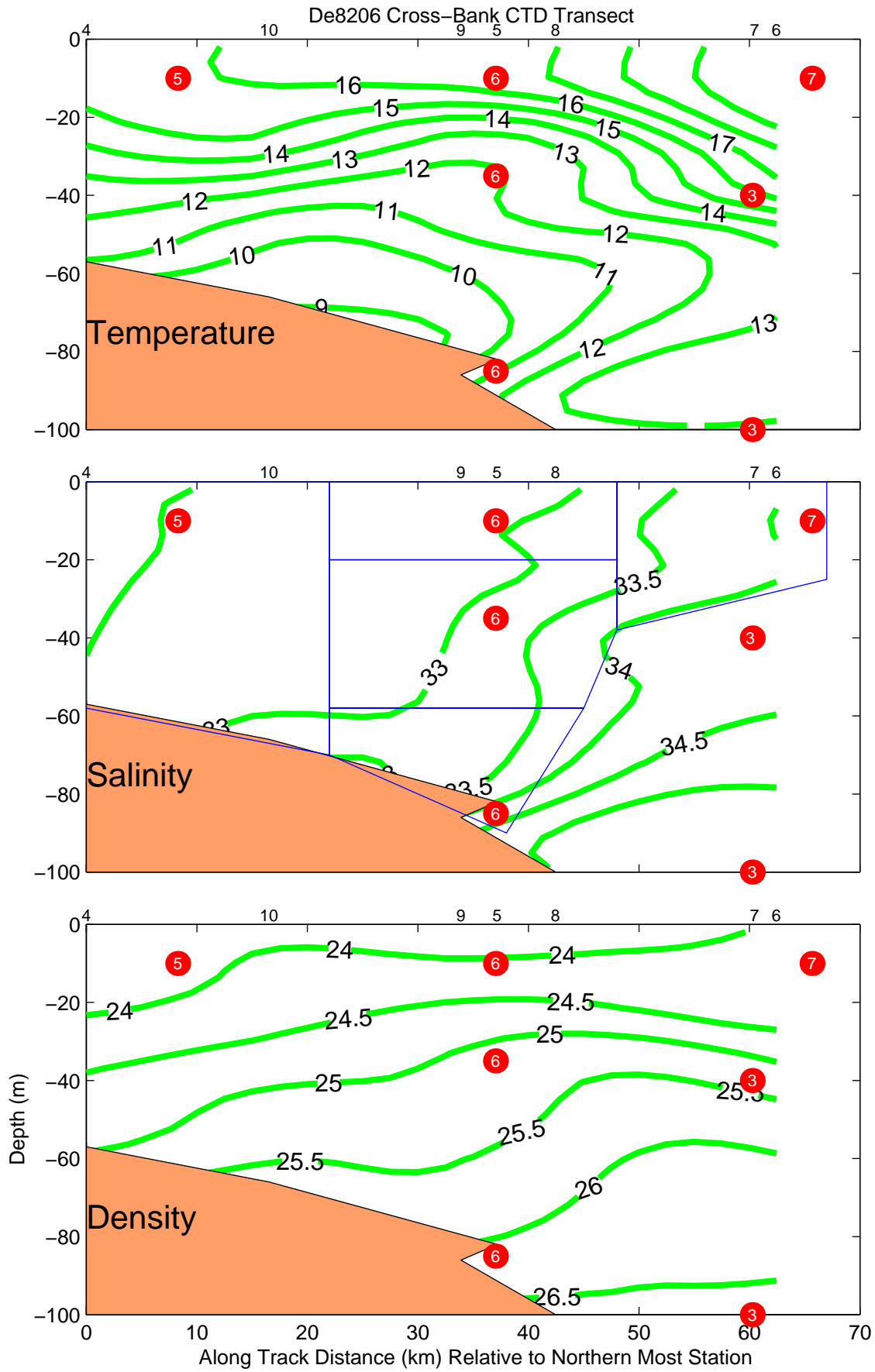
16 August 1982 at 0800Z



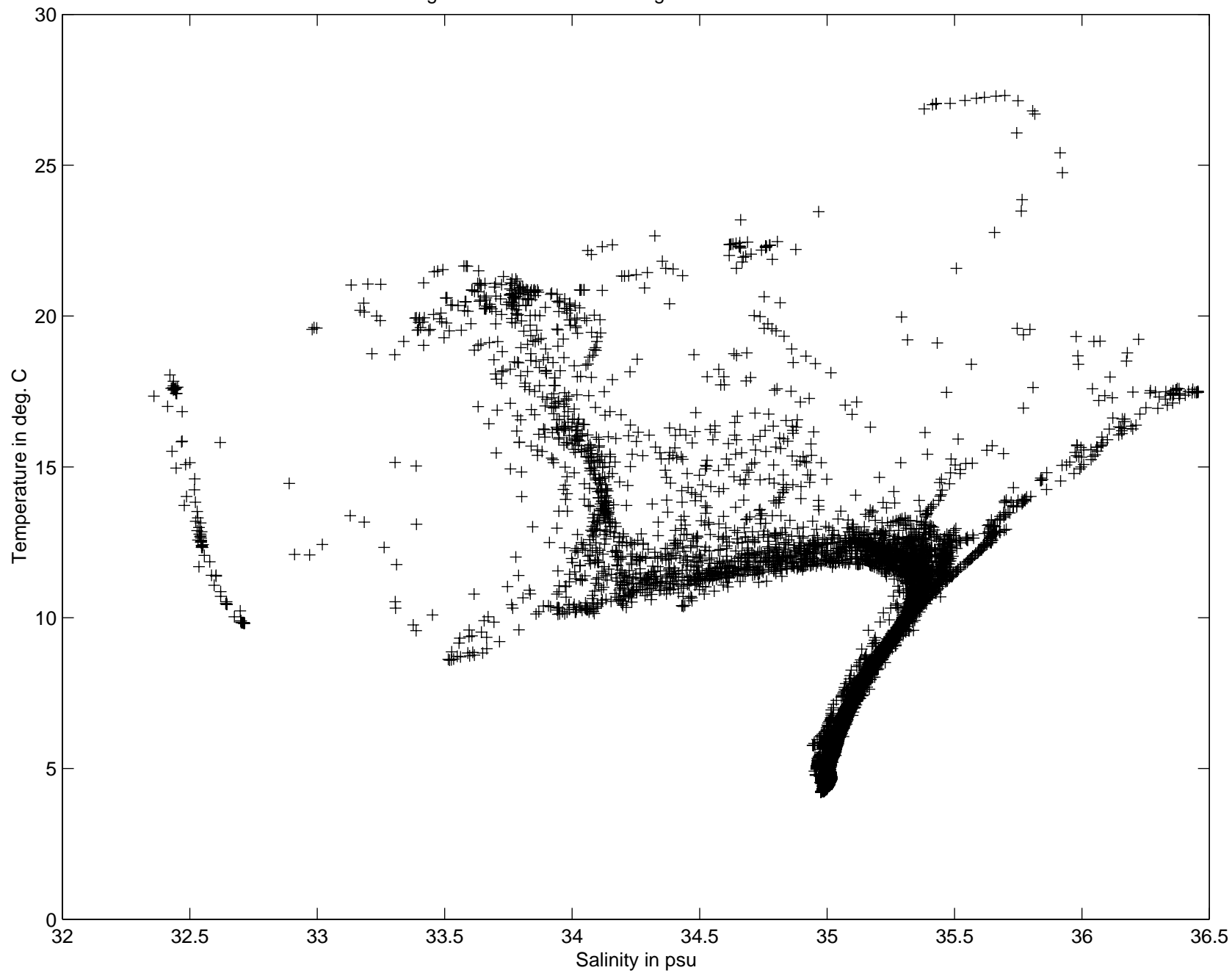


AL8209 Cross-Bank CTD Transect

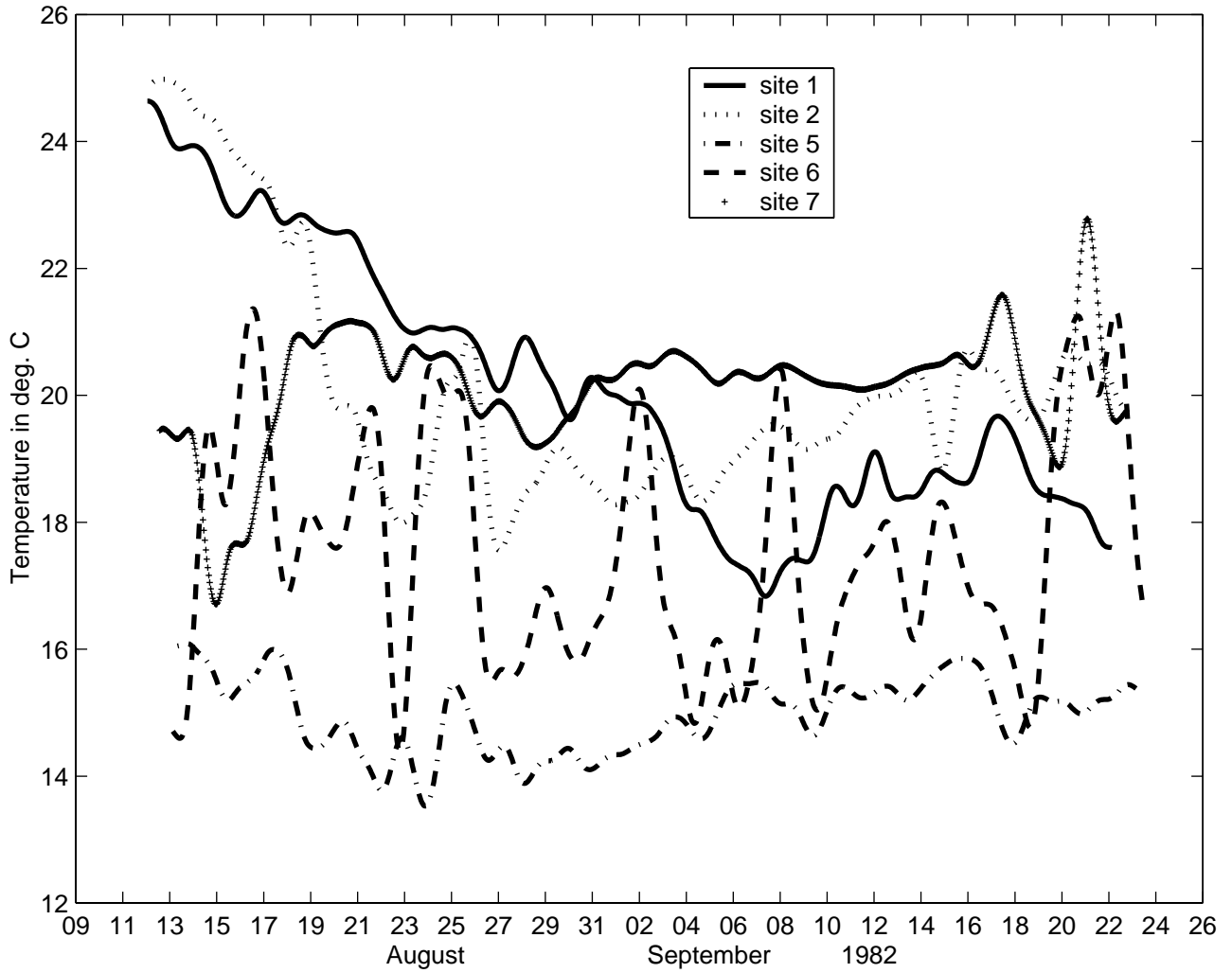




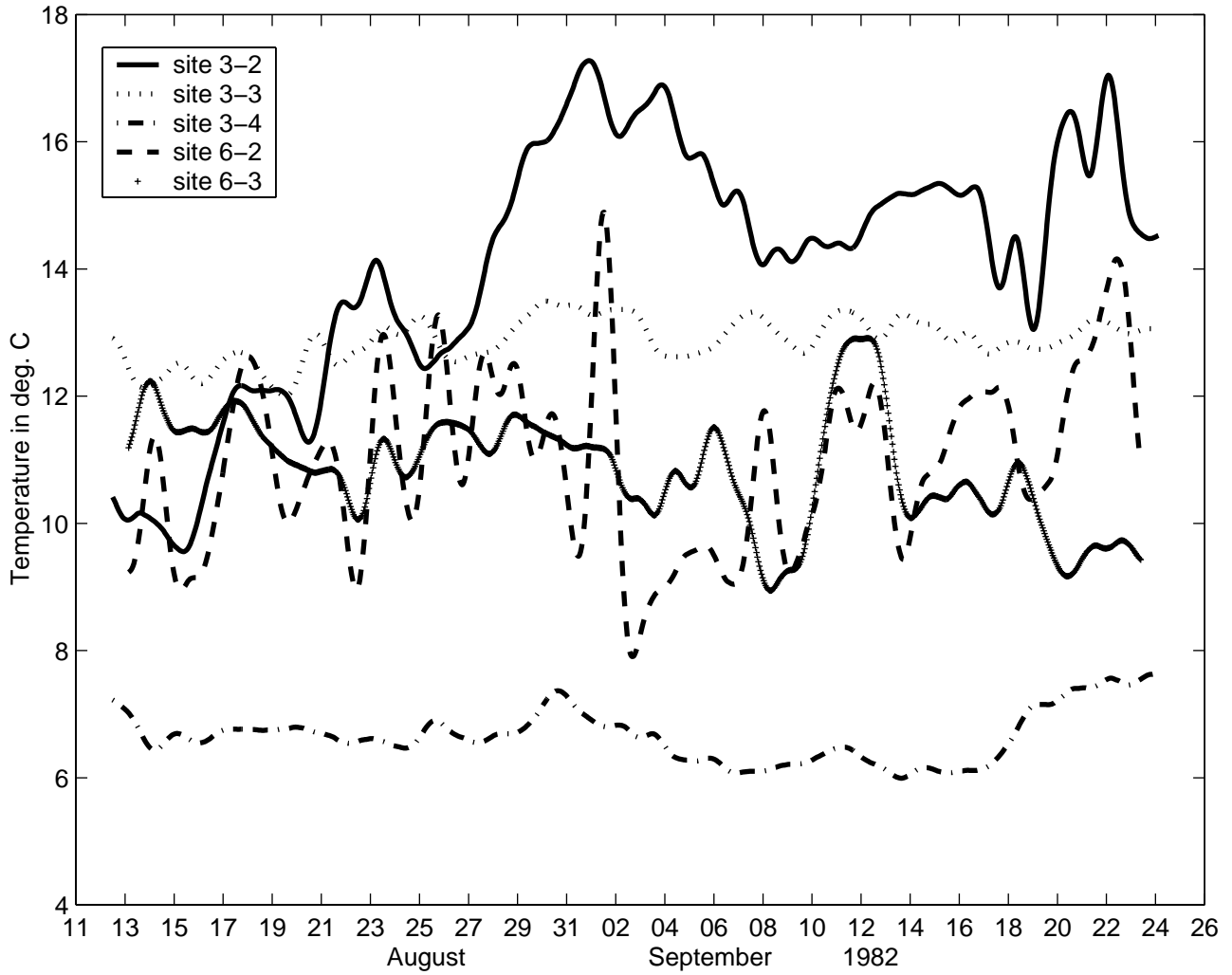
T-S diagram from CTD data during Ablatross IV cruise AL-8209



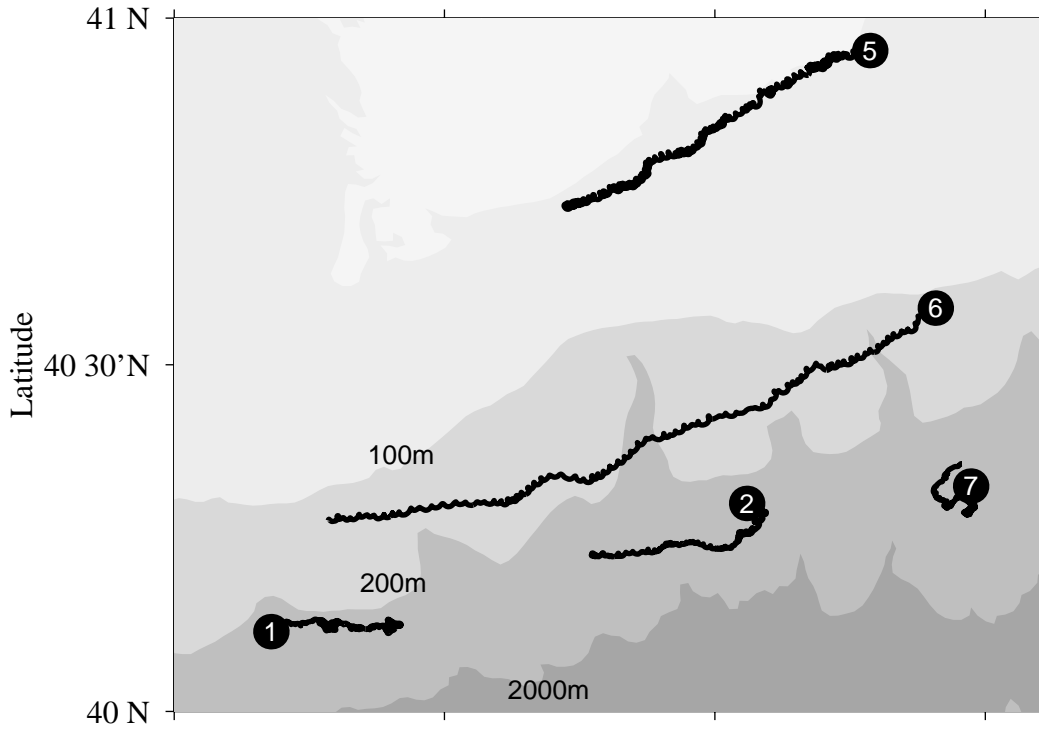
Temperatures at 10 m from current meters during WCR II



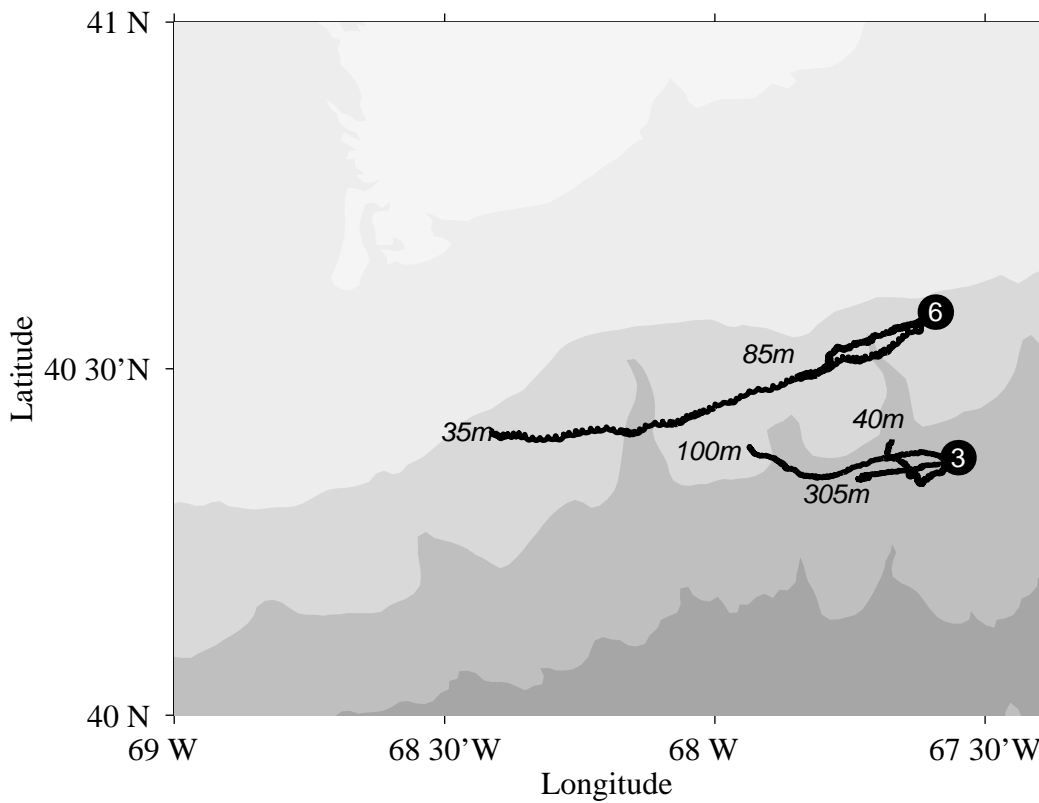
Temperatures at depths greater than 10 m from current meters during WCR II



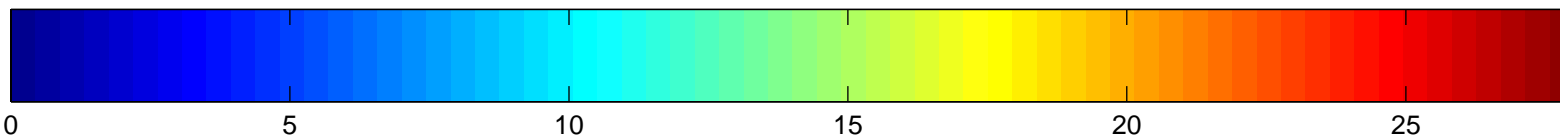
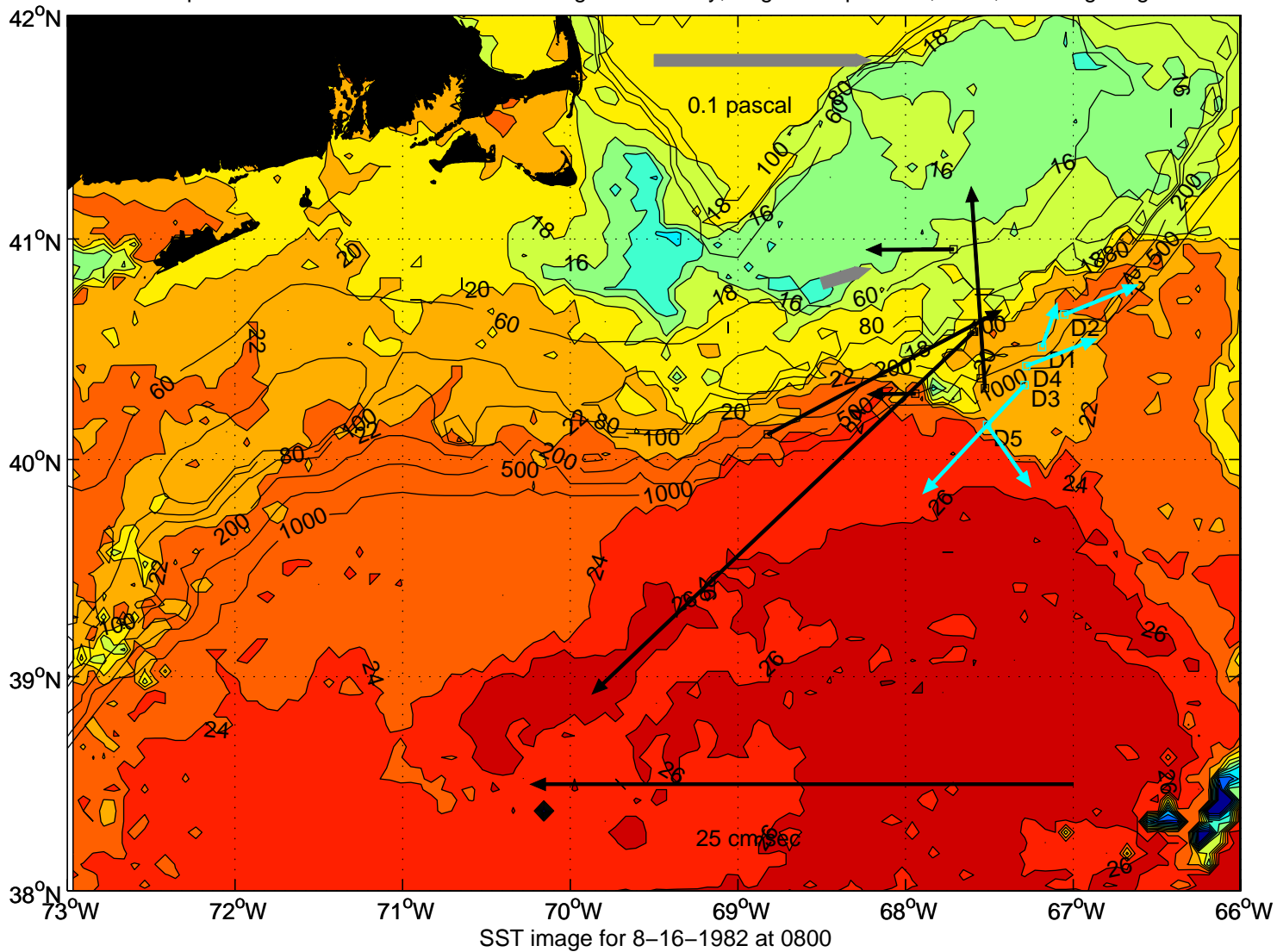
Advection at 10m

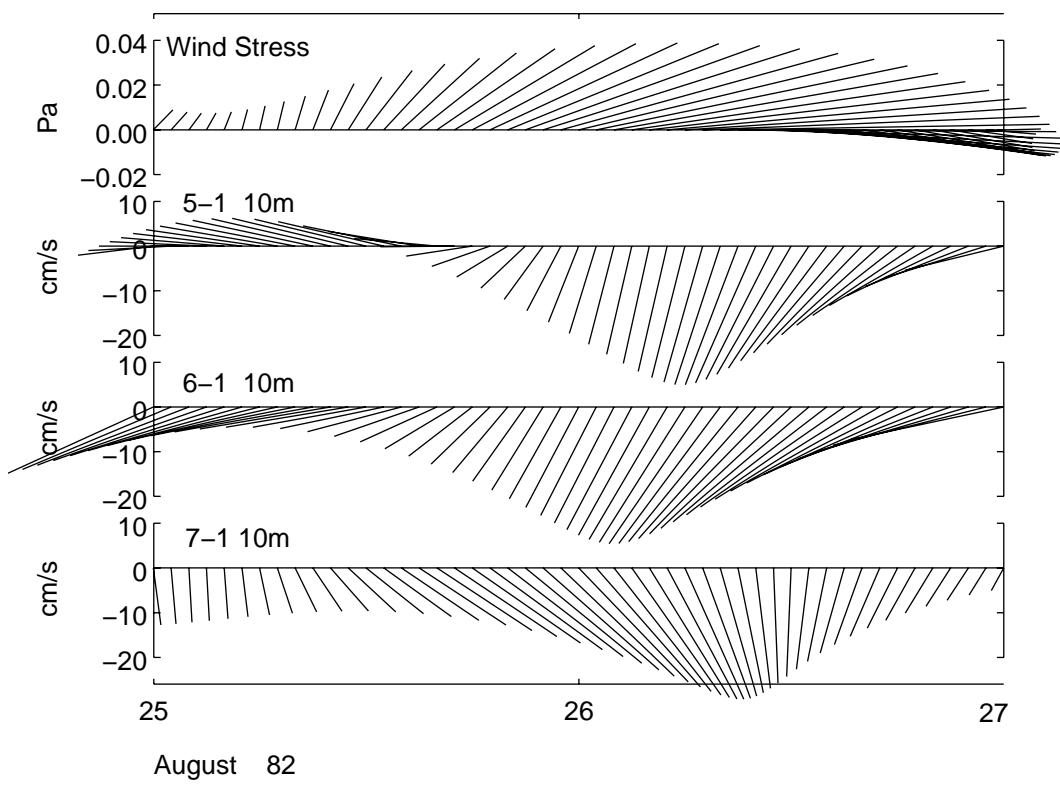


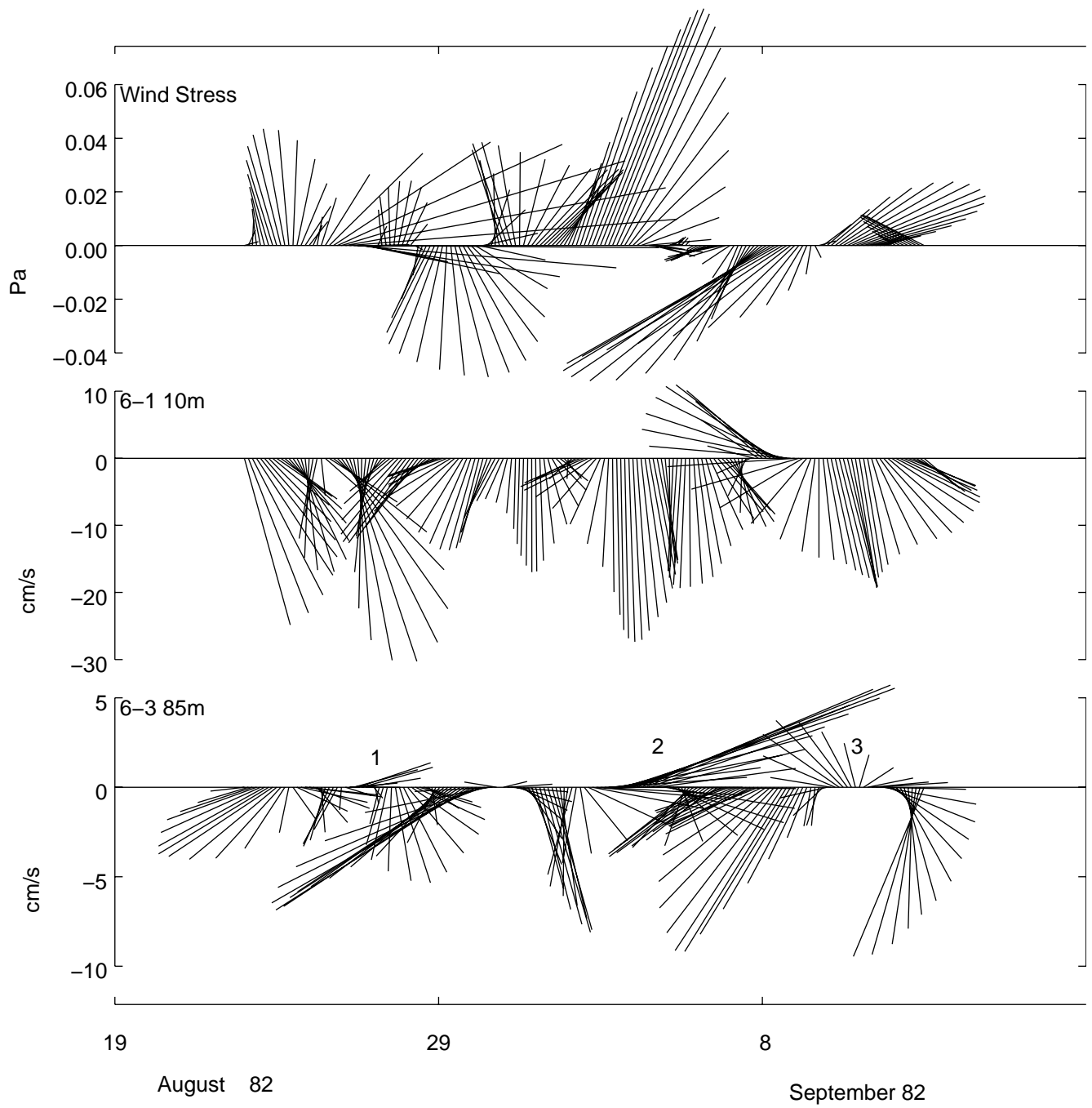
Advection greater than 10m

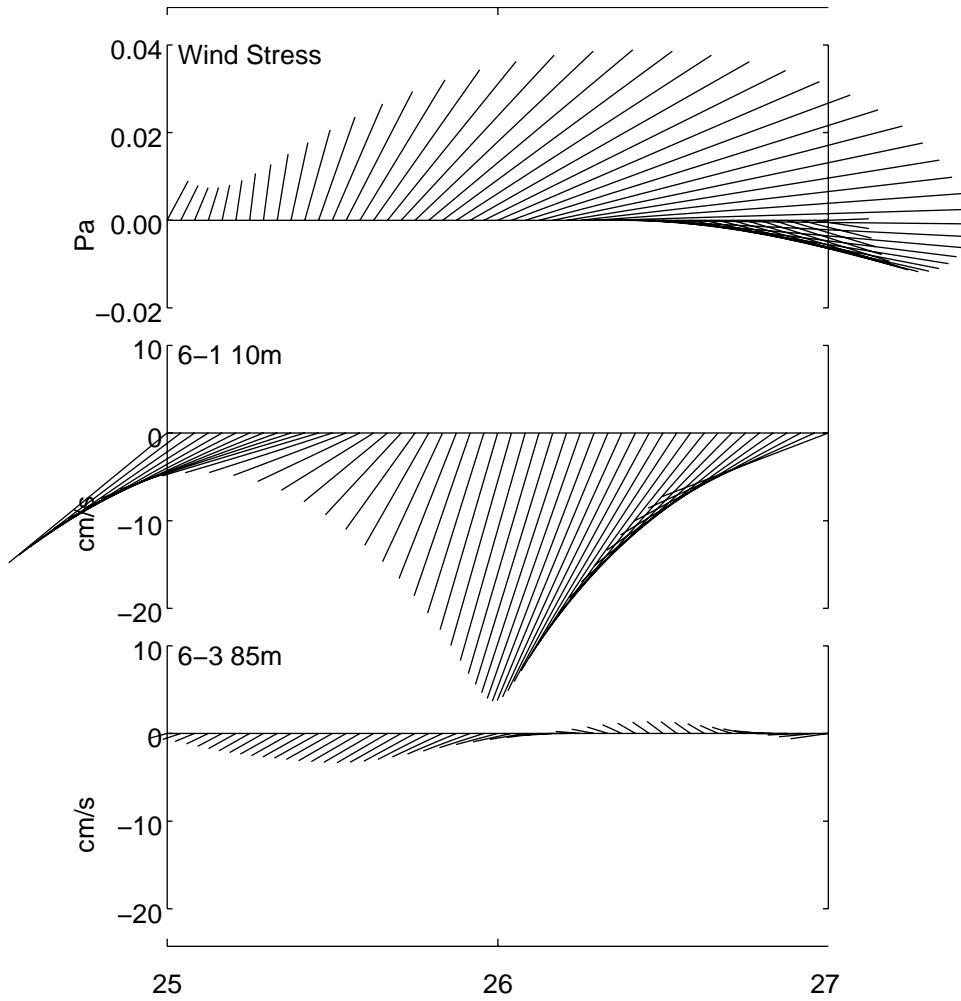


Low-passed currents and wind stress during WCRII array, August–September, 1982, including drogues

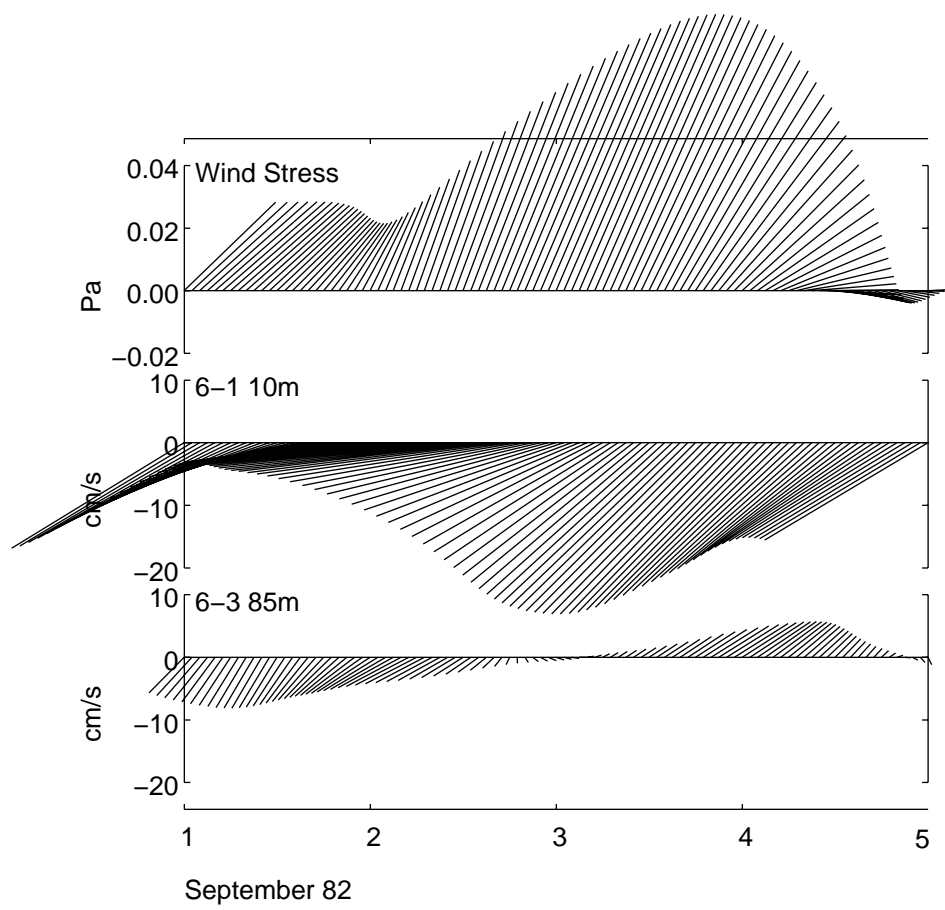


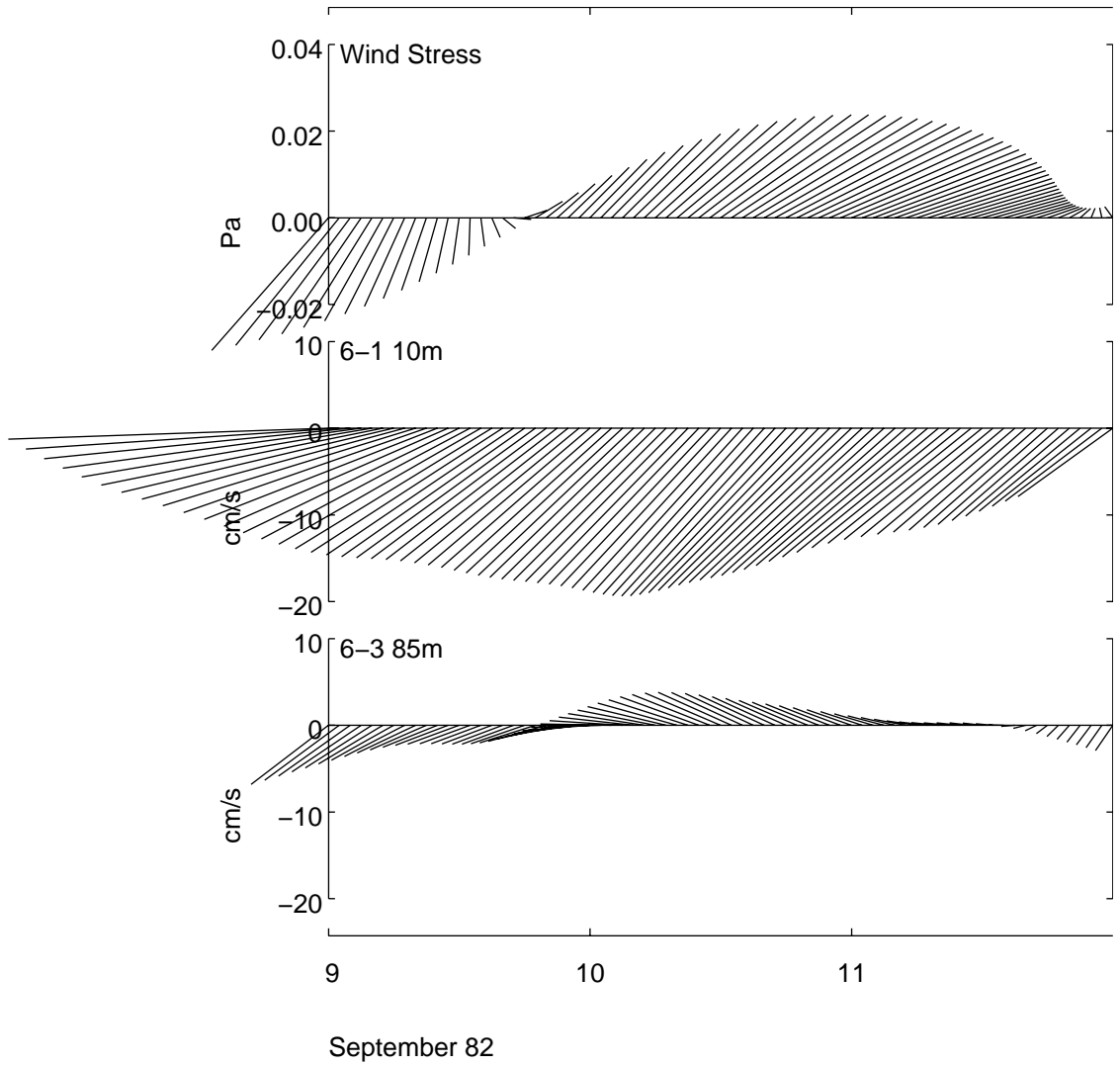


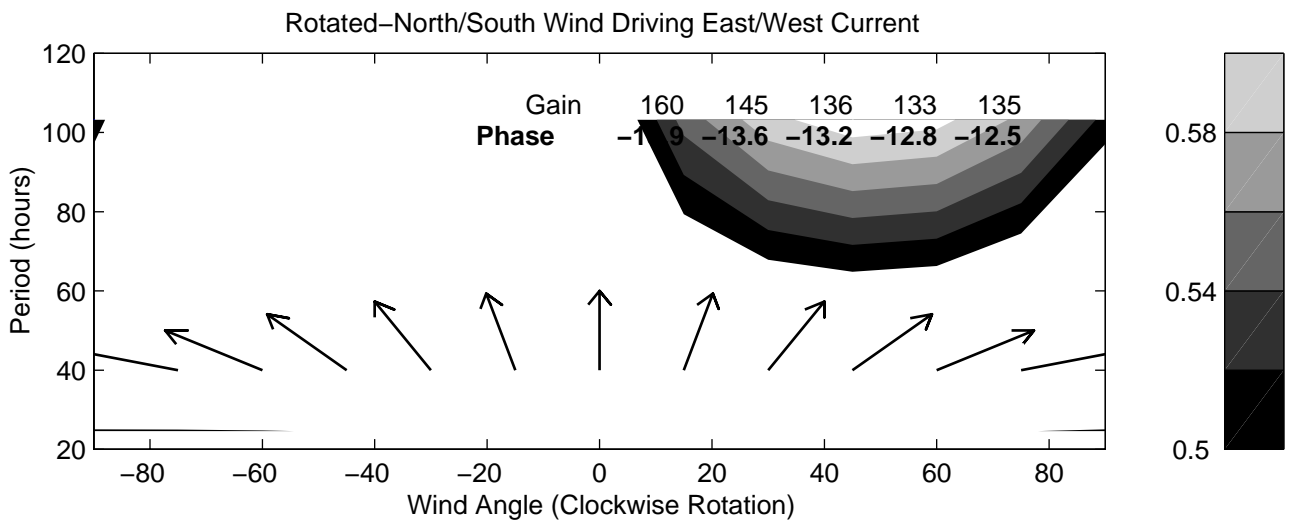
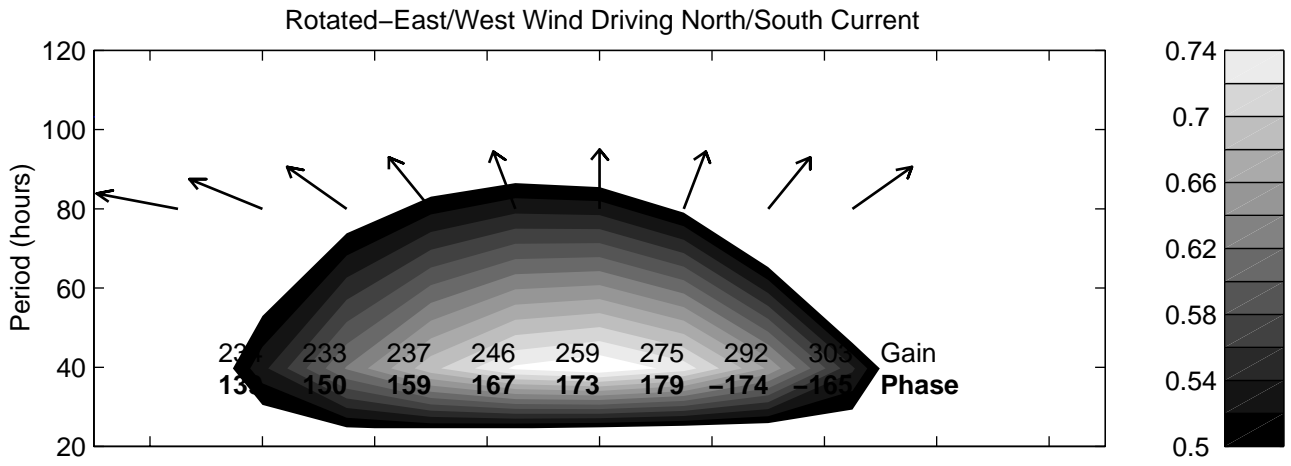




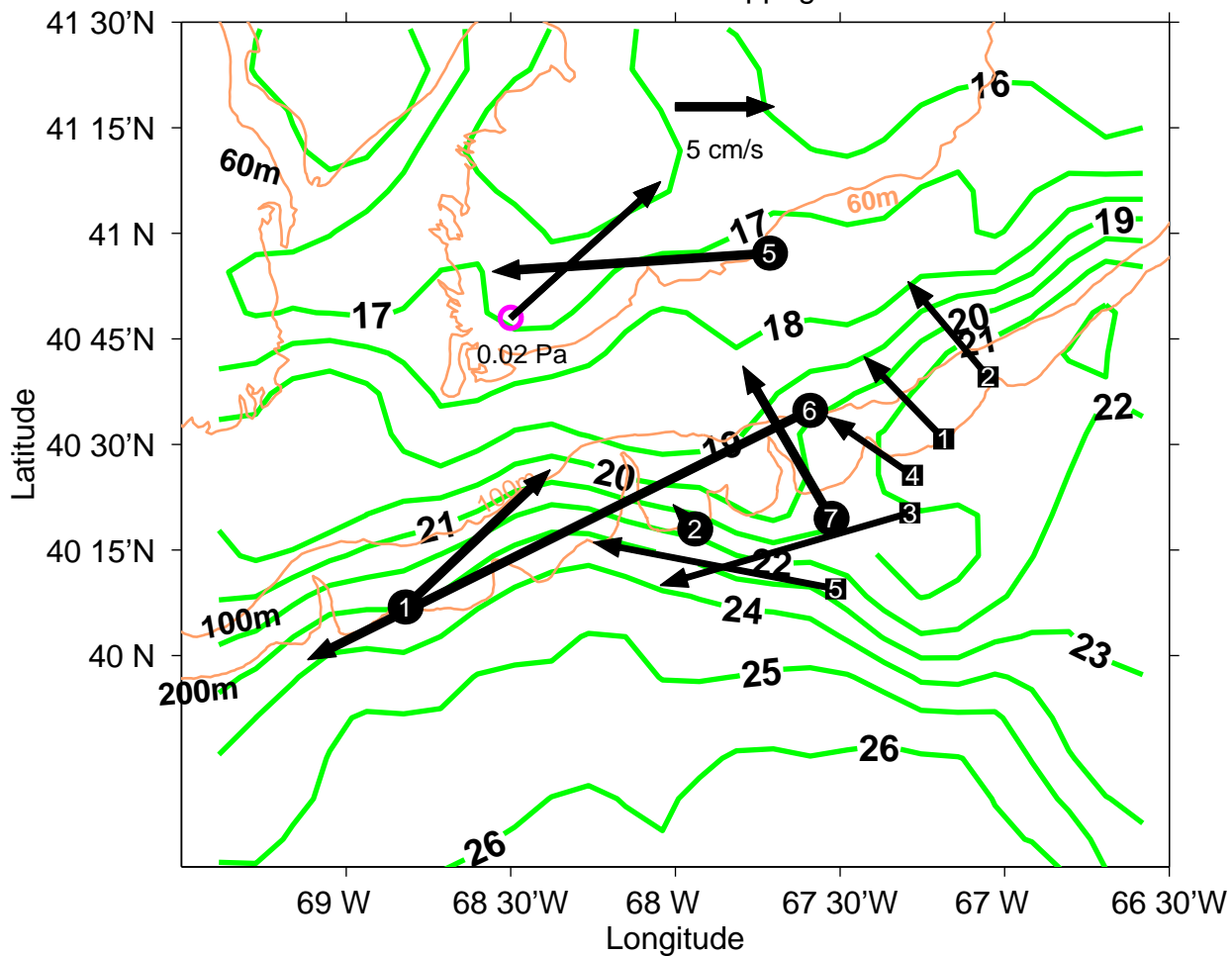
August 82



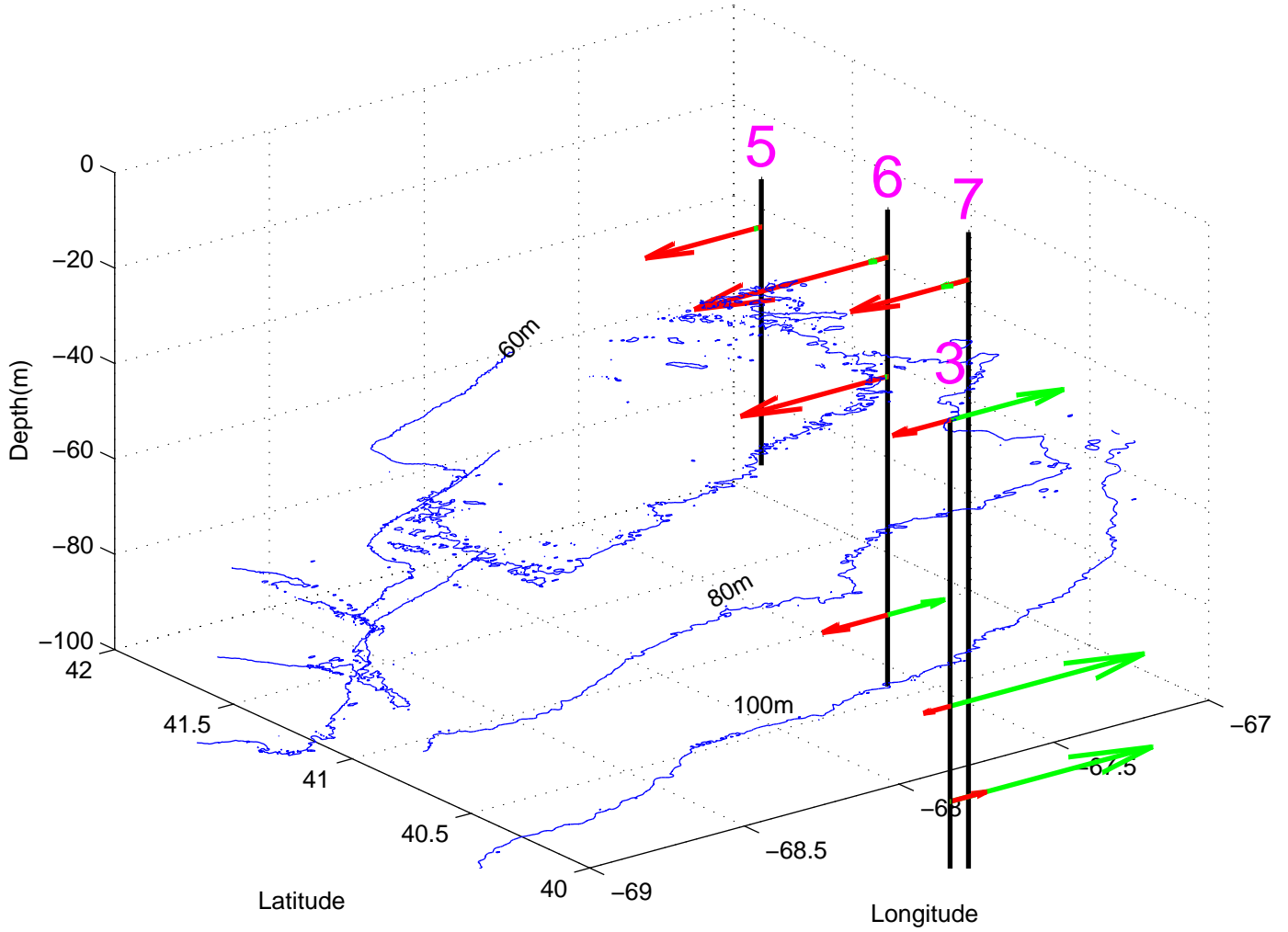


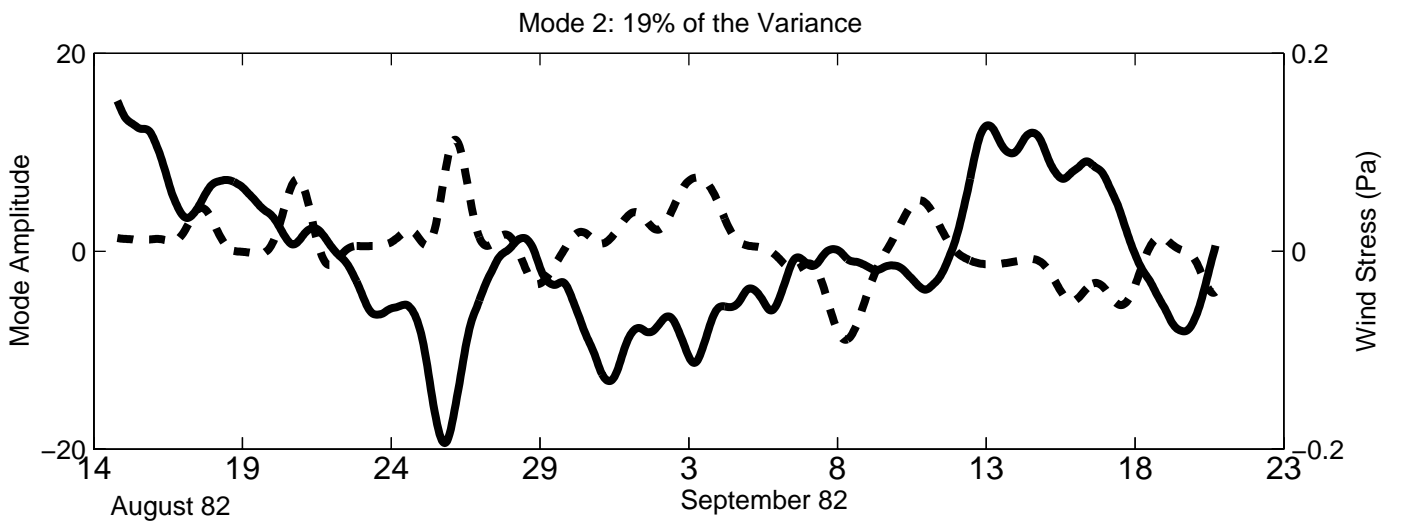
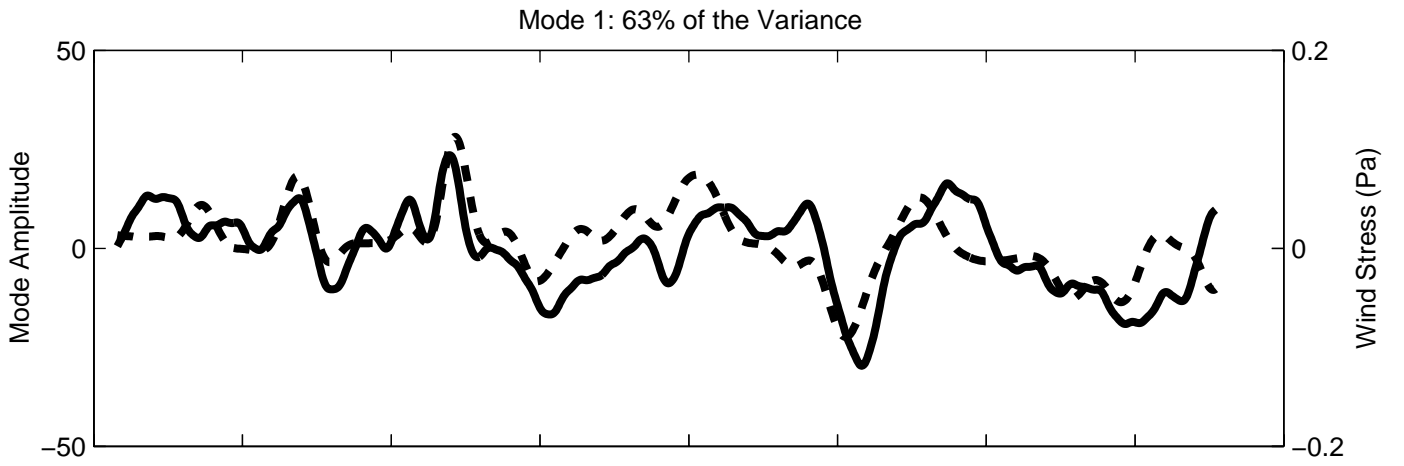


Wind-Driven Current & Slippage Removed



Mode 1 (red) and 2 (green)

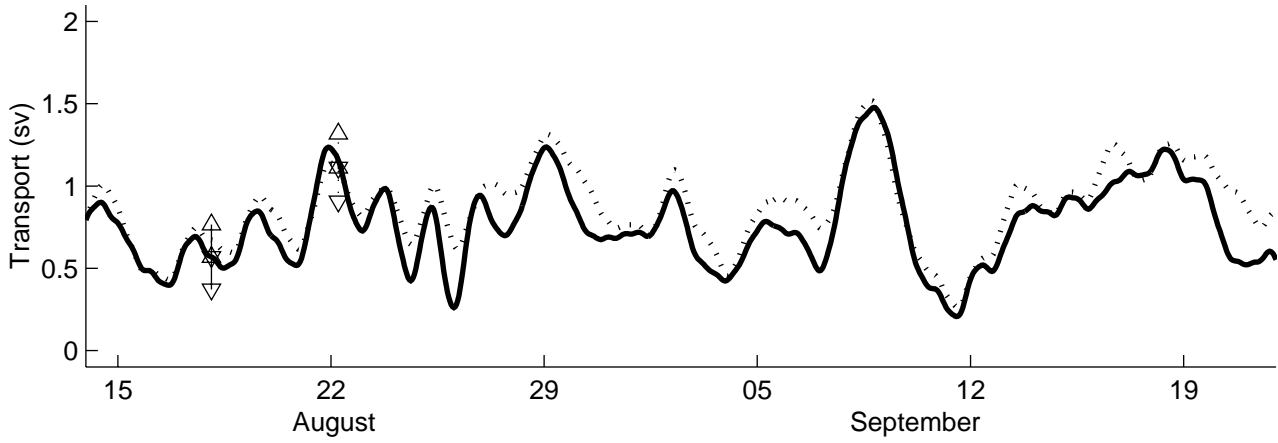




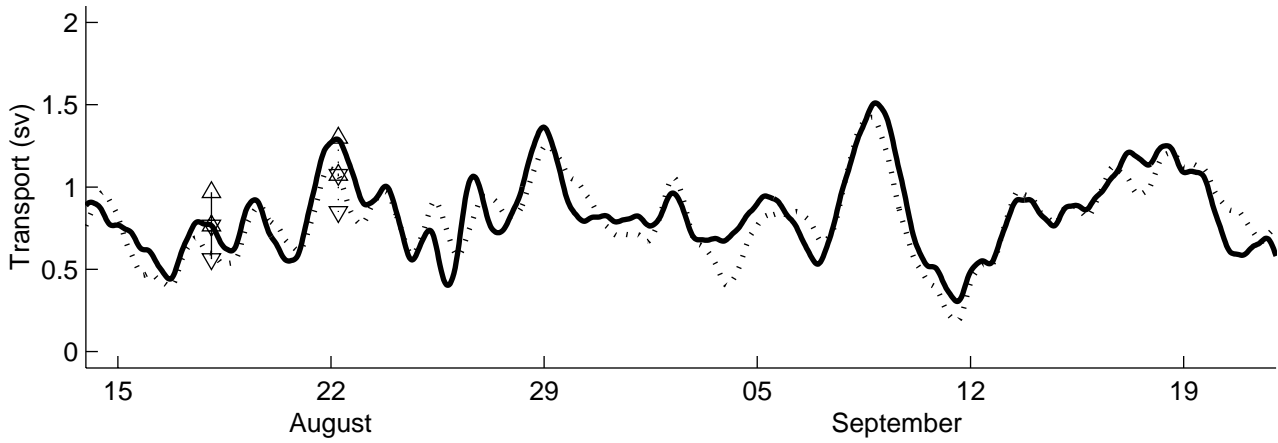
Case 1, August 1982



Estimated westward transport

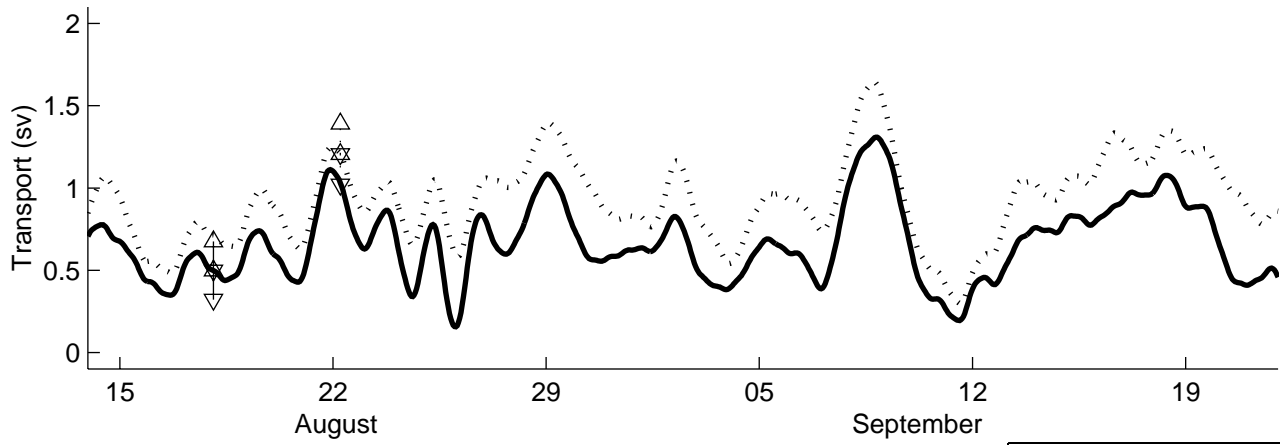


Estimated transport in direction of mean velocity

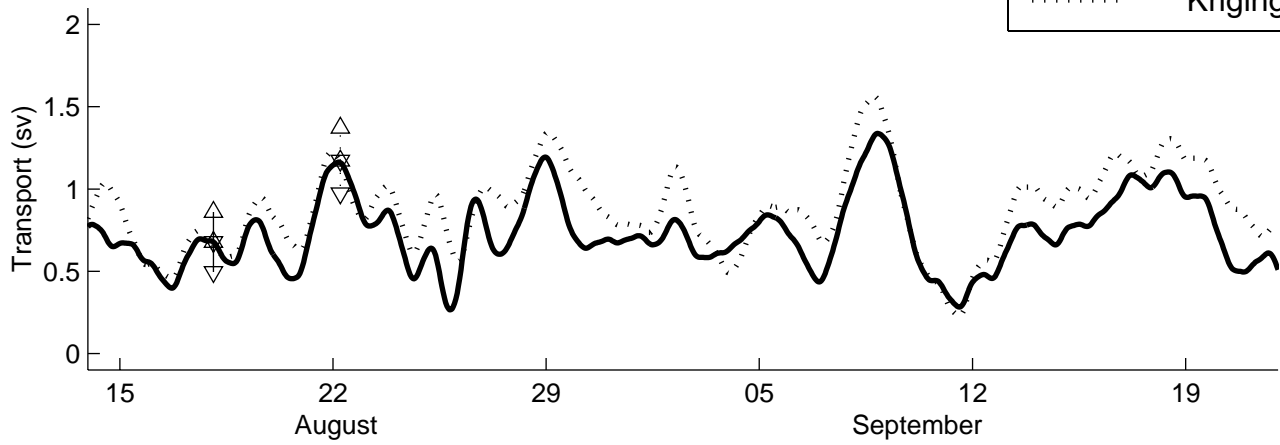


Case 2, September 1982

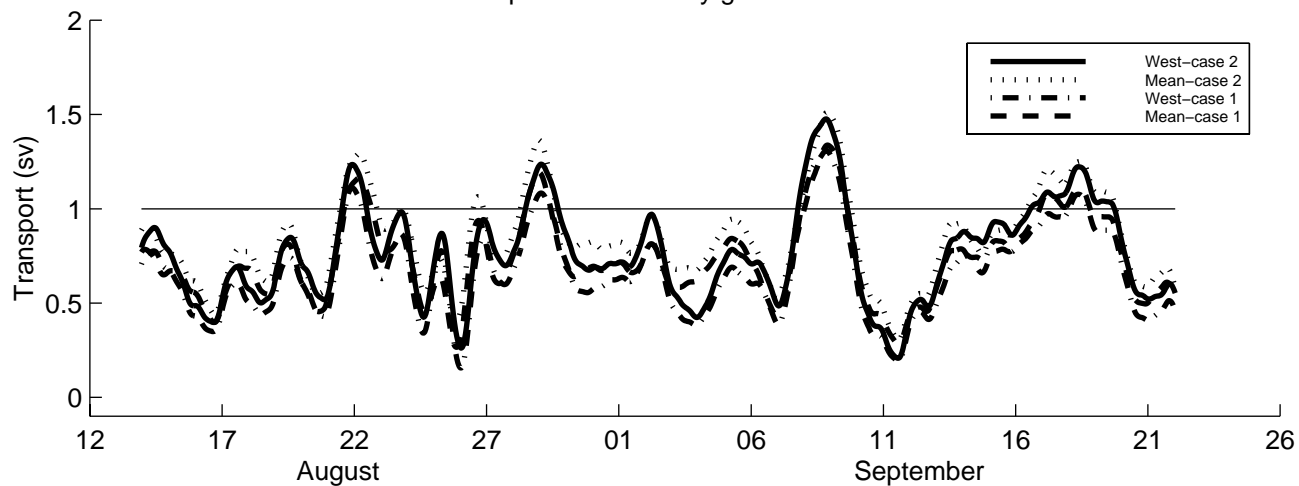
Estimated westward transport



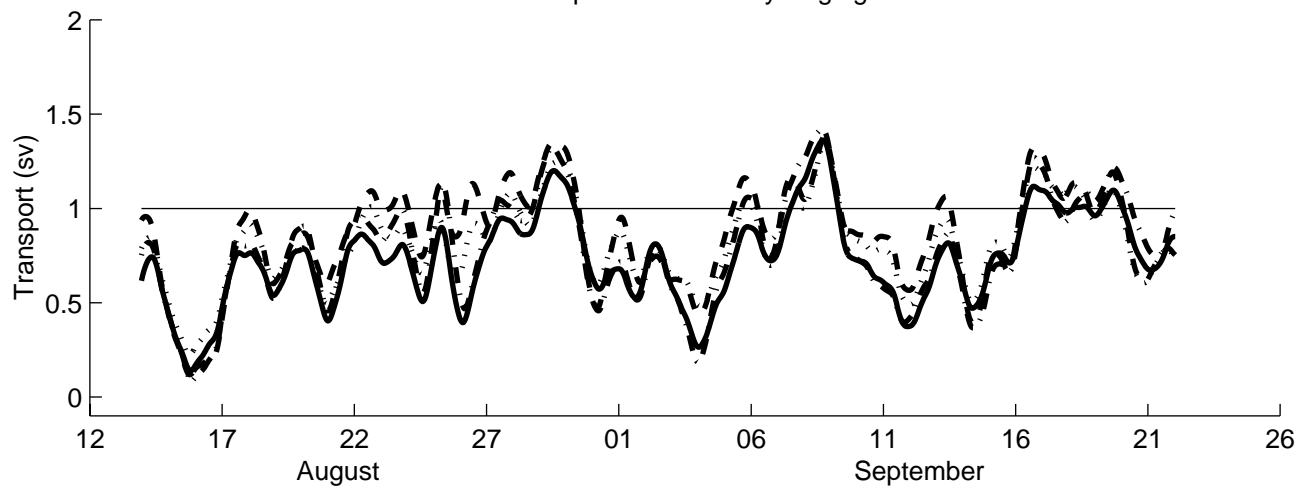
Estimated transport in direction of mean velocity



Transport estimated by geometric method



Transport estimated by Kriging



Estimated westward transport

